Heliyon 9 (2023) e13985

Contents lists available at ScienceDirect

Heliyon

journal homepage: www.cell.com/heliyon

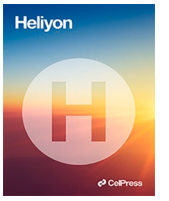

Research article

Translational characterization of the temporal dynamics of metabolic dysfunctions in liver, adipose tissue and the gut during diet-induced NASH development in Ldlr−/−.Leiden mice

Eveline Gart [a,b,*], Wim van Duyvenvoorde [a], Jessica M. Snabel [a], Christa de Ruiter [a], Joline Attema [a], Martien P.M. Caspers [c], Serene Lek [d], Bertie Joan van Heuven [e], Arjen G.C.L. Speksnijder [e], Martin Giera [f], Aswin Menke [a], Kanita Salic [a], Kendra K. Bence [g], Gregory J. Tesz [g], Jaap Keijer [b], Robert Kleemann [a], Martine C. Morrison [a]

[a] Department of Metabolic Health Research, The Netherlands Organization for Applied Scientific Research (TNO), 2333 CK Leiden, the Netherlands
[b] Human and Animal Physiology, Wageningen University, 6708 WD Wageningen, the Netherlands
[c] Department of Microbiology and Systems Biology, The Netherlands Organization for Applied Scientific Research (TNO), Zeist, the Netherlands
[d] Clinnovate Health UK Ltd, Glasgow, United Kingdom
[e] Naturalis Biodiversity Center, Leiden, the Netherlands
[f] Center for Proteomics and Metabolomics, Leiden University Medical Center, Leiden, the Netherlands
[g] Pfizer Worldwide Research, Development & Medical, Internal Medicine Research Unit, Cambridge, MA, USA

ARTICLE INFO

Keywords:
Non-alcoholic fatty liver disease
Temporal dynamics
Inter-organ crosstalk
Oxidative stress
Liver fibrosis

ABSTRACT

Background: NAFLD progression, from steatosis to inflammation and fibrosis, results from an interplay of intra- and extrahepatic mechanisms. Disease drivers likely include signals from white adipose tissue (WAT) and gut. However, the temporal dynamics of disease development remain poorly understood.

Methods: High-fat-diet (HFD)-fed Ldlr−/−.Leiden mice were compared to chow-fed controls. At t = 0, 8, 16, 28 and 38w mice were euthanized, and liver, WAT depots and gut were analyzed biochemically, histologically and by lipidomics and transcriptomics together with circulating factors to investigate the sequence of pathogenic events and organ cross-talk during NAFLD development.

Results: HFD-induced obesity was associated with an increase in visceral fat, plasma lipids and hyperinsulinemia at t = 8w, along with increased liver steatosis and circulating liver damage biomarkers. In parallel, upstream regulator analysis predicted that lipid catabolism regulators were deactivated and lipid synthesis regulators were activated. Subsequently, hepatocyte hypertrophy, oxidative stress and hepatic inflammation developed. Hepatic collagen accumulated from t = 16 w and became pronounced at t = 28–38 w. Epididymal WAT was maximally hypertrophic from t = 8 w, which coincided with inflammation development. Mesenteric and subcutaneous WAT hypertrophy developed slower and did not appear to reach a maximum, with minimal inflammation. In gut, HFD significantly increased permeability, induced a shift in microbiota composition from t = 8 w and changed circulating gut-derived metabolites.

* Corresponding author. The Netherlands Organization for Applied Scientific Research (TNO), Zernikedreef 9, 2333 CK Leiden, the Netherlands.
E-mail address: eveline.gart@tno.nl (E. Gart).

https://doi.org/10.1016/j.heliyon.2023.e13985
Received 29 November 2022; Received in revised form 17 February 2023; Accepted 17 February 2023
Available online 24 February 2023

Conclusion: HFD-fed Ldlr−/−.Leiden mice develop obesity, dyslipidemia and insulin resistance, essentially as observed in obese NAFLD patients, underlining their translational value. We demonstrate that marked epididymal-WAT inflammation, and gut permeability and dysbiosis precede the development of NAFLD stressing the importance of a multiple-organ approach in the prevention and treatment of NAFLD.

1. Introduction

Non-alcoholic fatty liver disease (NAFLD) is the most prevalent form of chronic liver disease worldwide. It is estimated to affect more than 20% of the adult population and is also becoming increasingly prevalent in children [1]. The pathophysiology of NAFLD is incompletely understood, which may contribute to the fact that at present no approved therapeutic treatments are available. NAFLD is the hepatic manifestation of the metabolic syndrome, characterized by visceral fat accumulation, hyperlipidemia and insulin resistance [2]. NAFLD is a complex multifactorial disease in which progression from simple steatosis to hepatic inflammation (non-alcoholic steatohepatitis; NASH) and fibrosis is driven by an intricate interplay between many molecular and cellular mechanisms [1]. These are not limited to the liver, where processes such as lipid accumulation, inflammation and oxidative stress are potential disease drivers, but also originate from other key metabolic organs such as the adipose tissue and the gut [3]. Current knowledge of the disease pathogenesis is based largely on studies that investigate a single time point (typically end-stage disease). However, such studies provide no insight into the temporal disease dynamics and chronology, which therefore remain poorly understood.

NAFLD is thought to begin with the accumulation of hepatic lipids, a condition known as steatosis. Hepatic lipids start to accumulate when the rates of lipid uptake and production exceed the rates of lipolysis and subsequent oxidation in peroxisomes and mitochondria, and lipid export (via VLDL). The excessive lipid load in the liver of NAFLD patients has been associated with increases in specific bioactive lipids such as diacylglycerols (DAGs) [4] - which can directly affect insulin signaling [5,6] - and byproducts of oxidative-stress-induced lipid peroxidation [7]. These metabolic dysfunctions can induce hepatocellular damage and may contribute to hepatic inflammation (infiltration of mixed inflammatory cells along with increases in proinflammatory cytokines and chemokines) [8], as well as hepatic fibrosis.

In addition to metabolic dysfunction in the liver of NAFLD patients, growing evidence suggests that the development of NAFLD is closely linked to the dysfunction of other metabolic organs, in particular the gut and adipose tissue [9]. For example, NAFLD patients have an altered microbiota composition [10] and increased gut permeability [11]. This altered microbiota composition may change nutrient processing, resulting in an altered production of short-chain fatty acids and bile acids, which can impact hepatic signaling pathways and metabolism [12]. In obesity-associated NAFLD visceral fat has important clinical implications and is an independent risk factor of the metabolic syndrome [13,14]. White adipose tissue depots in obese subjects can become inflamed and can thus contribute to NAFLD, via lipid overflow which increases the lipid load on the liver, or via secretion of inflammatory cytokines and adipokines.

However, it is unclear when specific pathogenic events in the liver itself, and in gut and adipose tissue occur, what the sequence of these events is, and how they relate to NAFLD development (e.g., whether increased gut dysfunction precedes WAT dysfunction and NASH or whether the various organ dysfunctions develop simultaneously with NASH). Recent NAFLD research has mainly focused on the late stage of disease (e.g., fibrosis), however to prevent severe disease development more attention should be paid to the early phase of disease. For the latter, translational models for NASH in which the early phase of disease development and potential biomarkers can be studied play an important role. Advancing our understanding of processes underlying NASH pathogenesis, the organ interactions and the complex interplay between them is crucial for the development of effective therapies.

Therefore, in this study we investigated temporal dynamics of metabolic dysfunctions in multiple organs (liver, adipose tissue, gut) during NAFLD development to investigate organ crosstalk. In particular, the sequence of pathogenic events as well as relevant metabolites released by these organs were studied. Knowledge on the disease dynamics will help define key pathogenic mechanisms and identify factors formed in these tissues that associate with fatty liver progression towards NASH and fibrosis. To study this we performed a longitudinal study to allow the study of both NASH (expected around 28 weeks) and liver fibrosis (evident around 38 weeks) as endpoint in the Ldlr−/−.Leiden mice. Ldlr−/−.Leiden mice display characteristics akin to NASH patients confirmed on the histopathological [15], metabolomic [16,17] and transcriptional level [17,18]. Ldlr−/−.Leiden mice develop NAFLD in the context of obesity, hyperlipidemia with a humanized lipid profile, and hyperinsulinemia when fed energy-dense diets with a macronutrient composition comparable to natural human diets, thus eliminating the need to artificially modify the diets by adding cholesterol or lowering the methionine or choline content [18–20]. A group of mice were euthanized at start point (t = 0 weeks) and after 8, 16, 28 (NASH endpoint) and 38 weeks (liver fibrosis endpoint). At these time points features of HFD-induced metabolic dysfunction in liver, adipose tissue and the gut during NAFLD development were evaluated and compared with low-fat diet controls. Metabolic dysfunctions in the Ldlr−/−.Leiden mouse model were compared to those observed in NASH patients, to further assess the translational value of this NASH mouse model.

2. Materials and methods

2.1. Animals

Male Ldlr−/−.Leiden mice were bred and housed in the AAALAC-accredited SPF animal facility at TNO Metabolic Health Research

(Leiden, the Netherlands). These mice are a substrain of the commercially available Ldlr−/− mouse (The Jackson Laboratory) and have a 94% C57BL/6J background and 6% 129S1/SvImJ background. The animals were used herein for a time course experiment in accordance with the rules and regulations set forward by the Animal Care and Use Committee and with ethical approval from an independent Animal Welfare Body (IVD TNO; approval number 3682/TNO-245). In addition, all procedures performed on these animals were in accordance with regulations and established guidelines and were reviewed and approved by Pfizer Institutional Animal Care and Use Committee. The mice were group-housed (four to five mice per cage) in Macrolon type 2L cages in a clean-conventional animal room (relative humidity 55 ± 10, temperature 20–24 °C, light cycle 07:00 to 19:00) with ad libitum access to food and water. From weaning onwards all mice (n = 103) were fed a standard laboratory low-fat control diet (chow; Sniff-R/M-V1530, Uden, the Netherlands). All mice were around the age of 14–16 weeks when the study started, and a group of these mice (n = 6) was euthanized as a starting reference group (t = 0). The remaining mice were divided into two different treatment arms, one part remained on chow while the others were fed an energy-dense high-fat diet (HFD; D12451, Research Diets Inc.; 20 kcal% protein, 35 kcal% carbohydrate mainly from sucrose and 45 kcal% lard fat) to induce NAFLD. 5 h-fasted blood samples for EDTA plasma preparation were collected from the tail vein at set intervals. Body weight and food intake measurements and body composition analyzed with echoMRI were acquired throughout the study. A few days before euthanasia, a functional gut permeability test was performed (details described below). Groups of n = 6 chow and n = 15 HFD fed mice were euthanized after 8, 16 and 28 weeks, and groups of n = 15 chow and n = 15 HFD fed mice after 38 weeks. Mice were euthanized by gradual-fill CO2 asphyxiation after a 5-h fast in the morning. At euthanasia blood for EDTA plasma and serum preparation was collected via heart puncture, organs were isolated and weighed, and mucosal microbiota from ileum and colon was collected. In addition, we included data from recent comparable studies using the same experimental conditions: male Ldlr−/−.Leiden mice of the same age fed the same diets (e.g. Ref. [20]).

2.2. Blood chemistry

Analysis of cholesterol, triglycerides, insulin, adiponectin and leptin, alanine amine transferase (ALT), aspartate aminotransferase (AST), CK-18M30 and TIMP1 in EDTA plasma and whole blood glucose was performed as described previously [21,22]. 5-hours fasting plasma insulin and fasting blood glucose values were used to calculate IR = [insulin (ng/mL) × glucose (mM)]/22.5 [23]. At t = 20 weeks lipoprotein profiles were analyzed by separating plasma lipoproteins in fractions with fast protein liquid chromatography (FPLC) using (Pharmacia, Roosendaal, the Netherlands), as previously described [24]. In the plasma fractions total cholesterol and triacylglycerols were measured with enzymatic assays (Roche diagnostics, Basel, CHF) [24]. We also measured ApoB concentrations (t = 24 w) by ELISA following manufacturer instructions (ab230932, Abcam, Cambridge, UK). Gut-derived metabolites short-chain fatty acids (SCFAs; acetic acid, propionic acid, butyric acid, caproic acid, isobutyric acid, methylbutyric acid, isovaleric acid, and valeric acid) and bile acids (cholic acid, glycocholic acid, taurocholic acid, deoxycholic acid, taurodeoxycholic acid, chenodeoxycholic acid, β-muricholic acid, taurochenodeoxycholic acid, ursodeoxycholic acid, tauroursodeoxycholic acid, and hyodeoxycholic acid) were measured in 5-h-fasted terminal plasma at Triskelion (Utrecht, the Netherlands) as reported in Ref. [23].

2.3. Liver analyses

Liver histopathology was scored by a board-certified pathologist in Hematoxylin-Eosin (HE)-stained 3 μm cross sections of the medial lobe using a standardized method for rodents that is based on the human NAS scoring system [15]. Total steatosis (macrovesicular and microvesicular) and hypertrophy (abnormally enlarged hepatocytes) for each mouse were determined as a percentage of total liver section affected. Hepatic inflammation was quantified by 1) counting the number of inflammatory aggregates in 5 fields per mouse at 100× magnification (field of view 4.15 mm^2) and expressed as the number of aggregates per mm^2 in the HE liver cross sections and 2) counting the number of F4/80-positive CLS per 3 μm liver cross of the medial lobe, which were F4/80 immunohistochemically stained as detailed in Ref. [17].

Intrahepatic cytokines (IL10, IL17, TNFα) and chemokines (MIP1a/CCL3, IP10/CXCL10, RANTES/CCL5, KC/CXCL1) were measured as previously described in Ref. [25] using a Simoa multiplex immunoassay panel (3-plex 85-0450 and 4-Plex Developer Kit 100A-0497, Quanterix MA, USA) according to the manufacturer's protocol on an SP-X System (Quanterix). In the same liver homogenates cytokine MIF was measured following manufacturers protocol (Mouse MIF duoset DY1978, R&D systems, Abingdon, UK). Total protein concentrations were measured with the BCA Protein Assay Kit in the same homogenates (Thermo Fisher Scientific, Waltham, MA, USA) to normalize the inflammatory factors per mg of protein.

Hepatic fibrosis was analyzed in Sirius red-stained 3 μm cross sections of the sinister lobe and quantified by a board-certified pathologist as the percentage of hepatocytes affected. Hepatic total collagen content was quantified based on hydroxyproline residues obtained from acid hydrolysis (QZBtiscol, Quickzyme, Leiden, the Netherlands) of the sinister lobe. Collagen concentrations were normalized by protein concentrations, which were measured in the same hydrolysates (QZBtotprot, Quickzyme) according to manufacturer's instructions.

Fibrosis architecture was analyzed as detailed in Ref. [17] with multiphoton and second harmonic generation (SHG) imaging of hepatic collagen using a Genesis 200 imaging system and subsequent computer-assisted data analysis (HistoIndex, Singapore).

Liver vascular structures of mice fed a chow or HFD for 44 weeks were analyzed in the right and caudate liver lobe stained for 20 h in a 1% iodine and 70% alcohol solution. The iodine-enhanced vascular structures were visualized by Micro-CT scanning (Zeiss Xradia Versa 520 with Zeiss Scout-and-Scan software, Carl Zeiss B.V., Breda, the Netherlands). The subsequent settings were used: 0.4× objective, pixel size 28.147 μm and 24.16 μm (chow and HFD, respectively), voltage 40/3 kV/W, camera binning 2, 801 views and 1201 views (chow and HFD, respectively) with angle range of 180° + fan. Followed by 3D construction of the vascular structures with

Zeiss XMReconstructor software.

The oxidative stress marker 4-hydroxynonenal (4-HNE) was analyzed by immunohistochemistry in 4-HNE stained liver cross sections and quantified as previously described [26,27].

Liver lipids were analyzed with lipidomics on the lipidizer platform as detailed in Ref. [28].

Lipids were grouped into classes: cholesterol esters (CE), ceramides (CER), dihydroceramides (DCER), hexosylceramides (HCER), lactosylceramides (LCER), lysophosphatidylcholines (LPC), lysophosphatidylcholines (LPE), phosphatidylcholines (PC), phosphatidylethanolamines (PE), sphingomyelins (SM), free fatty acids (FFA), diacylglycerols (DAGs), triacylglycerides (TAGs). The concentrations of the lipids were expressed as nmol/mg tissue, the total abundance of each lipid class is the sum of the respective lipid species concentrations.

Next generation sequencing was performed in RNA samples extracted from n = 6 chow and n = 10 HFD animals at 38 weeks. RNA concentration and RNA quality were determined as previously reported [25]. RNA sequencing libraries for the Illumina (Ilumina NovaSeq6000, San Diego, CA) platform were generated Paired-End 150 bp for approximately 20 million Paired-End reads per sample at Genomescan BV (Leiden, the Netherlands). The sequences were filtered, trimmed and subjected to a QC procedure as described previously [29]. These files were then merged and aligned to the reference genome "Mus_musculus.GRCm38. gencode.vM19". Htseq-count 0.6.1p1 was used to count the reads, these count files served as input for the differentially expressed genes (DEGs) analysis using the DESeq2-method [30]. DEGs were used as an input for pathway analysis through Ingenuity Pathway Analysis (IPA), accessed 12/21 [31]. IPA uses gene expression data of all known downstream target genes to predict activation or deactivation of an upstream regulator as reported [22,29].

2.4. Adipose tissue analysis

The perigonadal WAT (gWAT) and mesenteric WAT (mWAT) visceral white adipose tissue depots and the inguinal subcutaneous WAT (iWAT) were isolated and weighed. All three depots were paraffin-embedded and cross sections (5-μm thick) were stained with hematoxylin-phloxine-saffron. Adipocyte morphometry (cell size and count) was analyzed using the automated image analysis plug-in Adiposoft [32] in ImageJ [33]. Inflammation was quantified by scoring the amount of crown-like structures (CLS) in the same fields as the morphometry analyses and expressed as number of CLS/1000 adipocytes as described in detail elsewhere [34].

2.5. Gut analysis

Gut permeability was assessed using a functional *in vivo* assay that measures the ability of fluorescein isothiocyanate (FITC)-labelled dextran (3–5 kDa FD4; Sigma, St. Louis, MO, USA) to cross from the intestinal lumen into the circulation as described previously [21]. A baseline blood sample was taken after a 4 h fast, then FD4 was administered by oral gavage (900 mg/kg). Four hours after FD4 administration a second plasma sample was collected to measure FD4 concentrations using a fluorometer (FLUOstar Galaxy, BMG labtech, Offenburg, Germany). The baseline blood sample was used to correct for autofluorescence.

Microbiota DNA was isolated from samples collected from the mucosa layer from both the ileum and the colon using the AGOWA mag mini kit (DNA Isolation Kit, AGOWA, Berlin, Germany) according to the manufacturer's instructions. Metagenomic sequencing of 16S rRNA gene (~270 bp), spanning the V4 hypervariable regions, and subsequent data analysis was performed as described previously [21].

2.6. Statistics

The present study tested the null hypothesis whether HFD feeding does not increase disease parameters relative to the lean chow controls. This hypothesis was tested for the respective HFD and chow groups at each time point [8, 16, 28 and 38 weeks). Statistical analysis was performed with IBM SPSS statistics version 25.0 (SPSS Inc., Chicago, Illinois, USA). Data was tested for normality with the Shapiro-Wilk test and for equal variance with Levene's test ($\alpha = 0.05$). Outliers were identified using robust regression and outlier removal (ROUT, with Q = 1%). For normally distributed variables, and independent sample *t*-test was used (1-sided). In case the data was not normally distributed, a Mann-Whitney test was used (1-sided). P-values < 0.05 were considered statistically significant. Correlations were studied by Pearson's correlation analysis. IPA analysis to determine differentially expressed genes were based on Fisher's exact test ($\alpha = 0.01$).

3. Results

3.1. HFD fed Ldlr−/−.Leiden mice develop features of the metabolic syndrome: obesity associated with increased visceral fat mass, hyperlipidaemia and hyperinsulinemia

As expected, HFD-feeding induced robust weight gain over the course of the 38-week diet study, inducing significantly increased body weight compared to chow fed mice already after 8 weeks. Fat mass was significantly elevated, primarily driven by an increase in visceral adiposity. Lean mass and caloric intake remained largely comparable between the two groups (Fig. 1A–C).

In chow-fed animals, the metabolic risk factors plasma cholesterol, triglycerides and insulin increased slightly over time while glucose and HOMA-IR remained stable (Fig. 1D–F). In contrast, HFD induced pronounced hyperlipidaemia as observed by a doubling of plasma cholesterol concentrations after 8 weeks that kept on rising until 28 weeks and then levelled-off. Plasma triglycerides showed

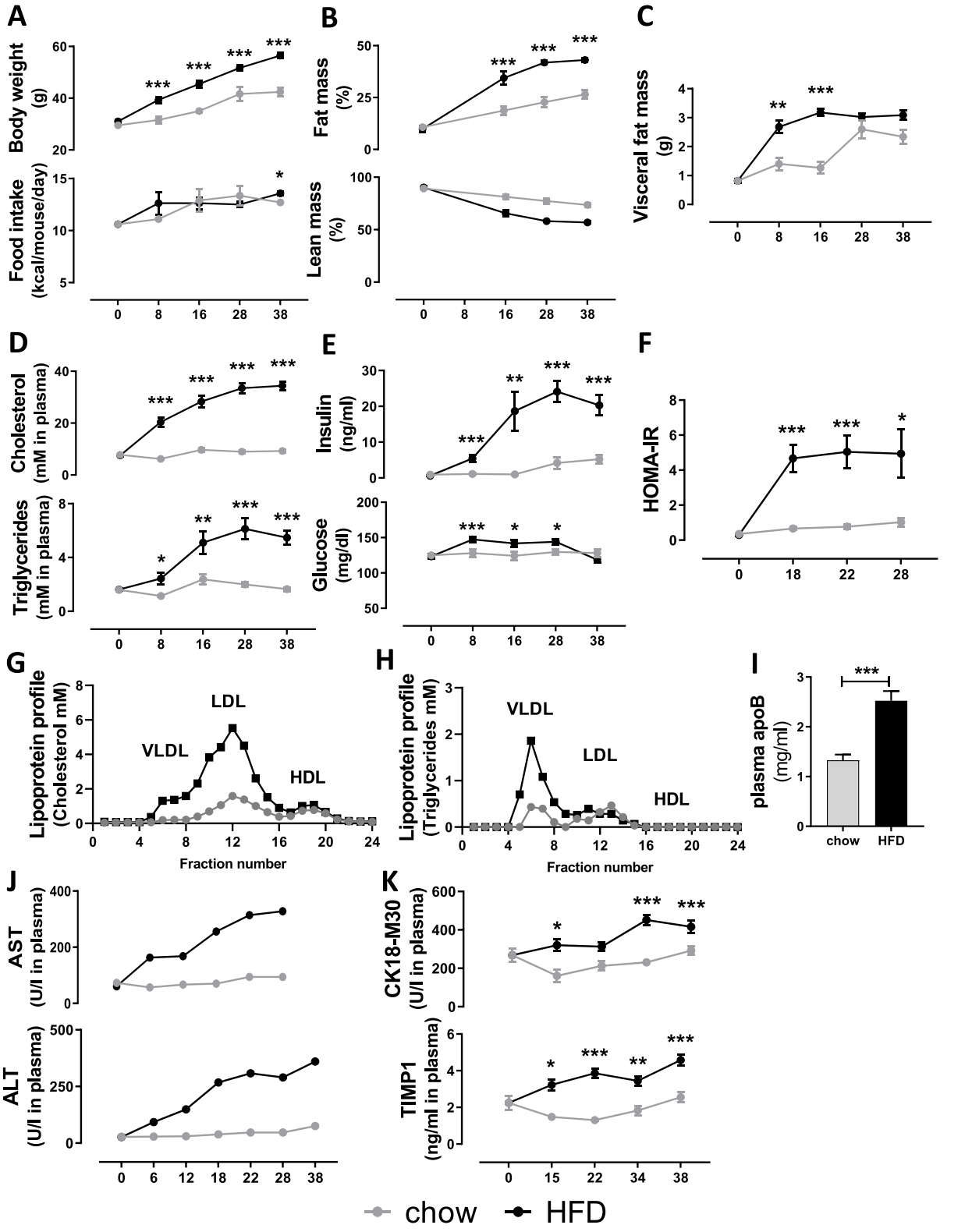

(caption on next page)

Fig. 1. Body composition, food intake and systemic metabolic parameters during NAFLD development. Groups of Ldlr−/−. Leiden mice fed a chow or a high-fat (HFD) diet were euthanized over time up to 38 weeks. (**A**) body weight and caloric food intake, (**B**) Fat mass and lean mass determined with echoMRI, (**C**) visceral fat mass is a composite of the visceral epididymal and mesenteric fat mass. In 5-h fasted plasma (**D**) cholesterol and triglyceride concentrations were determined as well as (**E**) insulin and glucose in whole blood. Insulin and glucose concentrations were used to calculate the (**F**) HOMA-IR. Lipoprotein profiles were analyzed in fasting plasma pools (n = 15/grp) and fractionated with FPLC, in the respective fractions (**G**) cholesterol and (**H**) triglyceride concentrations were determined at t = 20 and plotted as profiles. (**I**) plasma apoB concentrations. Circulating liver integrity markers (**J**) AST and ALT were determined in plasma pools (n ≥ 8/grp). Liver damage markers including (**K**) CK-18M30 and TIMP1 were analyzed in 5-h fasted plasma. The x-axis indicates the time in weeks and data represent mean ± SEM with * $p < 0.05$, ** $p < 0.01$, *** $p < 0.001$ vs. HFD.

a comparable pattern over time. The HFD-induced increases in plasma cholesterol and triglycerides are mainly confined to the atherogenic apoB-containing (V)LDL lipoprotein particles as can be appreciated from the lipoprotein profiles in Fig. 1G–H essentially as observed in dyslipidemic humans [35,36] and in subjects with NASH [37]. In line with this, circulating apoB plasma concentrations were significantly increased by HFD relative to chow (Fig. 1I).

HFD feeding induced pronounced hyperinsulinemia after 8 weeks and fasting insulin levels continued to rise and were four-fold higher than chow at 38 weeks. Glucose levels remained similar over time in both chow and HFD animals. Together with the high insulin concentrations, this indicates a pronounced decrease in systemic insulin sensitivity with HFD. Consistent with this, HOMA-IR as a measure of insulin resistance was also found to be significantly increased with HFD.

The liver damage markers ALT and AST in plasma (Fig. 1J–K), routinely used as clinical liver function markers, were determined on the group level demonstrating low levels in chow while in HFD they gradually continued to increase. Consistent with this, plasma concentrations of the liver integrity marker CK18-M30 and the liver fibrosis marker TIMP1 slightly increased with chow over time whereas HFD feeding significantly increased both biomarkers.

These data indicate that HFD-induced obesity is associated with an early (t = 8 weeks) increase in visceral fat mass, development of dyslipidemia and hyperinsulinemia, accompanied by an increase in circulating ALT, AST, CK-18 and TIMP1 levels. The latter plasma markers are indicative of liver damage as is typically observed in NAFLD/NASH patients [38,39].

3.2. Obesity-associated NASH and liver fibrosis progression are associated with increases in intrahepatic cytokines and chemokines

To investigate the temporal development of liver dysfunction in more detail, histopathological analysis of NASH and liver fibrosis was combined with biochemical analysis of intrahepatic cytokines, chemokines and collagen content. Chow-fed animals developed minimal hepatic steatosis and hepatocellular hypertrophy, with these features being only observed to a small extent at the later timepoints, after 28 and 38 weeks (Fig. 2A–F). In contrast, HFD feeding resulted in pronounced development of total hepatic steatosis already from 8 weeks onwards (Fig. 2A–B), represented by equal increases in both micro- (Fig. 2C) and macrovesicular steatosis (Fig. 2D), and increased hepatocellular hypertrophy (Fig. 2E–F).

In addition, hepatic inflammation scored by histological quantification of the inflammatory aggregates and F4/80-positive crown-like structures (CLS) was practically absent in the chow fed-mice (Fig. 2G–J). HFD-feeding increased hepatic inflammation after 8 weeks, an effect which became pronounced after 16 weeks of HFD and kept rising both in the number of inflammatory cell clusters (Fig. 2G–H) as well as in the formation of F4/80-positive CLS (Fig. 2I–J). These hepatic CLS are a hallmark of NASH that has been shown to correlate with fibrosis development in NASH patients [40]. Histological observations of hepatic inflammation were supported by biochemical analysis of intrahepatic chemokines and cytokines (Table 1). HFD feeding induced increases in the pro-inflammatory cytokine IL-17 after 8 and 38 weeks, but did not significantly affect intrahepatic TNFα and MIF relative to chow. The chemokines CCL3, CCL5, CXCL1, CXCL10 on the other hand were all significantly increased by HFD feeding, and these chemokines are important for the infiltration of immune cells typically observed in NASH patients [41]. The anti-inflammatory cytokine IL-10 as potential counter-regulator response was significantly upregulated with HFD after 8 weeks and remained elevated at 16 weeks, though thereafter became comparable to chow levels.

In parallel, an NGS analysis and subsequent upstream regulator analysis was performed, which integrates changes in the expression of all known target genes downstream from a particular regulator. The upstream regulator analysis predicts the activity of an upstream regulator unrelated to its expression on protein level. HFD activated the pathways controlled by IL-17A, TNF, MIF, CCR2, CCL2 and CCL5 and IL-10 (Table 2). The activation of TNFα and MIF by HFD signaling was not associated with an increased hepatic protein expression of the respective cytokine/chemokine, which may be caused by downstream changes in signaling/activity.

Liver fibrosis was quantified by measuring the intrahepatic collagen content (Fig. 2K) and histologically by quantification of the Sirius-red (SR) positive area in liver cross-sections (Fig. 2L–M). The hepatic collagen concentrations and Sirius-red positive area remained low on chow diet. By contrast, HFD feeding induced liver fibrosis from 16 weeks onwards as observed by a doubling of the intrahepatic collagen content and an increased SR-positive area after 38 weeks. HFD feeding also induced changes in the fibrosis architecture over time as observed by significant increases in collagen area ratio, fiber density, reticulation index, number of fibers per area, mean fiber thickness and mean fiber length (Supplemental Fig. S1).

These data provide substantial context regarding the temporal development of NASH. Together this data indicates that the steep increase in body fat mass with HFD feeding is accompanied by an early accumulation of fat in the liver, followed by abnormal enlargement of hepatocytes. After 16 weeks, hepatic inflammation and hepatic collagen are slightly increased, and this becomes particularly prominent around the time hepatocyte expansion plateaus (28–38 weeks).

The comparison with mice on a chow diet shows that HFD-induced NASH and fibrosis results in profound changes in liver histology,

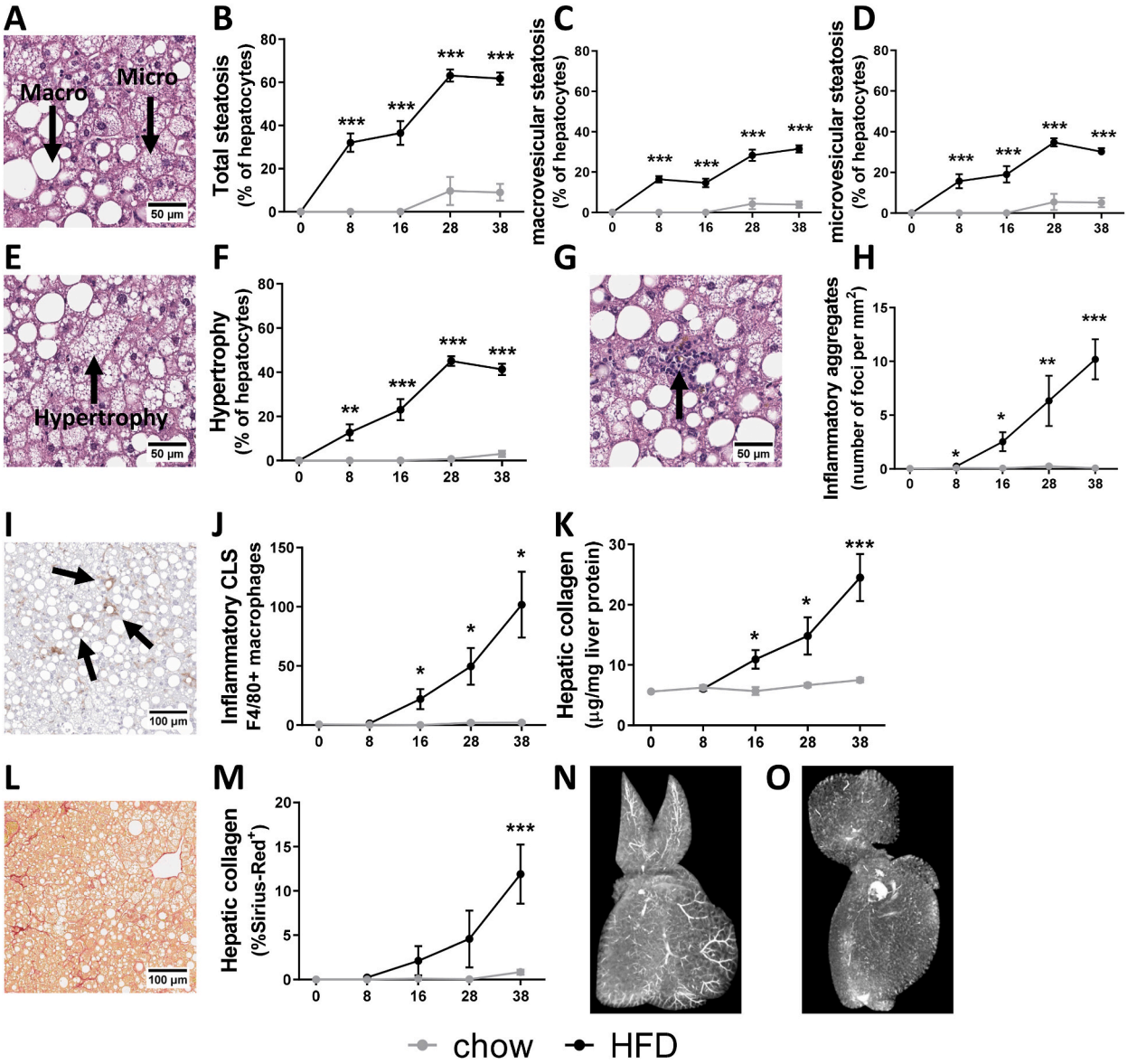

Fig. 2. Obesity-associated NASH and liver fibrosis development. (**A**) Illustrative picture of haematoxylin-eosin (HE) stained liver cross sections of HFD-induced NASH and scored for over time development of (**B**) total steatosis, a sum of (**C**) macrovesicular steatosis and (**D**) microvesicular steatosis. In the same HE cross sections (**E**) hepatocellular hypertrophy was (**F**) quantified. (**G**) Illustration of inflammatory aggregates (indicated by arrow) to score (**H**) hepatic inflammation of mixed inflammatory cell infiltration per mm^2, alongside analysis of (**I**) F4/80 immunoreactivity as marker of macrophages to score (**J**) inflammatory crown-like structures per cross section. Liver fibrosis was scored biochemically by quantification of (**K**) collagen content per mg protein and (**L**) histologically in Sirius-red stained liver cross-sections by (**M**) quantification of the percentage of Sirius-Red positive area. The x-axis indicates the time in weeks and data are presented as mean ± SEM. * $p < 0.05$, ** $p < 0.01$, *** $p < 0.001$ compared to the chow control group. Representative images from the 3D reconstruction supplemental videos of vascular structures analyzed by Micro-CT are demonstrated for (**N**) chow and (**O**) HFD.

suggesting an impact on the functionality and architectural characteristics of the organ. To illustrate this, livers from chow and HFD-treated mice were analyzed by Micro-CT followed by 3D reconstruction (Supplemental Video 1). This analysis showed that vascular structures, enhanced with iodine contrast, are clearly visible on a chow diet (Fig. 2N), while they were hardly visible anymore after HFD treatment (Fig. 2O), suggesting that the flow of blood and possibly also bile through the organ may be disrupted on a HFD.

3.3. NASH and liver fibrosis development associated with accumulation of specific lipids and the oxidative stress marker 4-HNE in the liver

As demonstrated by the histological analysis above, steatosis continuously increased during NAFLD progression. The accumulation

Table 1
Intrahepatic chemokines and cytokines concentrations.

	Chow					HFD			
	T=0	T=8	T=16	T=28	T=38	T= 8	T=16	T=28	T=38
IL-17	1.0	0.9	1.6	2.0	1.0	1.4	1.7	2.3	1.8
(pg/mg)	± 0.4	± 0.4	± 0.3	± 0.7	± 0.5	± 0.5	± 0.9	± 0.7	± 0.6
TNF-α	7.0	5.8	8.6	11.1	7.7	10.6	9.9	12.4	9.1
(pg/mg)	± 2.3	± 3.5	± 0.7	± 3.7	± 3.2	± 4.4	± 4.0	± 2.3	± 2.3
MIF	111.1	101.7	96.0	125.9	101.3	116.2	120.1	140.8	123.7
(ng/mg)	± 15.9	± 27.4	± 13.9	± 26.2	± 28.6	± 24.4	± 28.4	± 33.3	± 20.6
CCL3	1.0	1.6	1.3	2.1	2.2	2.6	9.7	12.6	19.6
(pg/mg)	± 0.2	± 1.2	± 0.1	± 1.1	± 1.4	± 1.5	± 11.3	± 8.3	± 8.3
CCL5	14.9	11.5	27.3	40.3	28.6	28.5	92.1	122.6	189.5
(pg/mg)	± 4.0	± 8.3	± 15.0	± 17.7	± 15.8	± 16.2	± 87.9	± 132.6	± 102.3
CXCL1	1.6	3.7	2.2	2.4	2.3	3.0	4.9	6.3	5.4
(pg/mg)	± 0.4	± 4.7	± 1.2	± 0.7	± 0.8	± 0.8	± 4.2	± 3.1	± 1.7
CXCL10	2.6	2.5	2.9	5.6	3.1	3.9	7.3	9.4	7.4
(pg/mg)	± 1.0	± 0.6	± 0.7	± 1.6	± 1.2	± 1.4	± 5.2	± 6.0	± 2.2
IL-10	15.8	16.3	18.7	27.5	19.3	24.3	25.5	30.0	24.7
(pg/mg)	± 4.6	± 5.7	± 2.8	± 6.5	± 8.9	± 6.3	± 10.1	± 6.5	± 6.5

IL-10 = Interleukin-10; IL-17 = Interleukin-17; TNF-α = tumor necrosis factor-α; MIF = macrophage migration inhibitory factor; MIP-1α = Macrophage inflammatory protein-1 alpha, also known as CCL3 = chemokine (C–C motif) ligand 3; RANTES = Regulated on Activation, Normal T cell Expressed and Secreted, also known as CCL5 = chemokine (C–C motif) ligand 5, KC = keratinocytes-derived chemokine, also known as CXCL1 = chemokine (C-X-C motif) ligand 1; IP-10 = interferon gamma-induced protein 10, also known as CXCL10 = chemokine (C-X-C motif) ligand 10. Data represents mean ± SD with significant differences between HFD and chow per time point ($p < 0.05$) were indicated in the HFD-fed groups, with significant increases shown in red.

Table 2
Upstream regulators involved in inflammation.

	HFD vs chow	
Upstream regulator	***Z-score***	***p-value***
IL10	1.6	0.000
IL17A	2.4	0.000
TNF	7.3	0.000
MIF	1.9	0.033
CCR2	5.0	0.000
CCL2	1.5	0.000
CCL3	-	-
CCL5	1.9	0.000
CXCL10	-	-

Upstream regulator analysis used gene expression data after 38 weeks of diet to predict the activity of an upstream regulator unrelated to its expression on protein level. The analysis integrates changes in the expression of all known target genes downstream from a particular regulator. The predicted activity of an upstream regulator is represented by a Z-score, a negative Z-score indicates inhibition of the respective regulator, and a positive Z-score indicates activation (shown in red). The p-value < 0.05 in grey indicates significant enrichment of the genes downstream of a regulator, i.e., that more downstream genes are affected than can be expected by chance. N/A indicates an insufficient number of differentially expressed genes to predict the activation state of an upstream regulator.

of lipids in liver is mostly attributable to a significant increase in TAGs: at start, approximately 15% of total liver fat were TAGs which increased to 70% of total liver fat at 38 weeks in HFD fed mice (Supplemental Fig. S2). In addition, HFD feeding also significantly increased the concentrations of the neutral lipids DAGs, CE and to some extend FFAs. In line with the HFD-induced increase of intrahepatic lipids and swelling of hepatocytes (steatosis & hypertrophy), the concentrations of intrahepatic phospholipids decreased: PC, PE, LPC, LPE, SM (Table 3), many of which are membrane lipids. The ceramide phospholipids HCER and LCER on the other hand,

were increased in HFD relative to chow.

Consistent with the development of steatosis in the HFD-fed animals, upstream regulator analysis predicted that important regulators involved in lipid catabolism (PPARA, AMPK, CLUH, SIRT1, UCP1), peroxisomal lipid catabolism (ACOX1) and mitochondrial biogenesis (PPARGC1A, PPARGC1B, ESSRA, NRF1, CLUH) were all inactivated with HFD feeding after 38 weeks (Table 4). At the same time, the activity of SREBF1, a positive regulator of fatty acid synthesis genes, was predicted to be activated with HFD, which is in line with the pronounced elevation of plasma insulin (which activates SREBF1). While TAG accumulation is considered a safe storage form of lipids, diacylglycerols (DAGs) block insulin signaling via protein kinase C (PRKC) at the level of the insulin receptor [42]. In line with the accumulation of DAGs the activity of protein kinase C delta (PRKCD) was also higher with HFD, indicating the development of lipid-induced hepatic insulin resistance essentially as observed in humans [5].

In NAFLD, a high lipid load can lead to increased lipid oxidation and subsequently higher rates of reactive oxygen species (ROS) production. When elevated, ROS production together with an impairment in antioxidant capacity can result in a redox imbalance and oxidative stress which is harmful for hepatocytes [43]. To understand the level oxidative stress in our model, the lipid peroxidation marker 4-HNE was longitudinally analyzed by immunostaining of liver cross-sections (Fig. 3). HFD feeding increased 4-HNE positive

Table 3
Intrahepatic lipid class concentrations.

	Chow					HFD			
	T=0	T=8	T=16	T=28	T=38	T=8	T=16	T=28	T=38
Neutral lipids									
TAG	11.8 ± 3.0	20.6 ± 10.9	19.3 ± 9.4	53.1 ± 35.7	43.1 ± 28.8	76.9 ± 27.8	132.4 ± 54.7	178.9 ± 33.3	156.6 ± 31.0
DAG	2.6 ± 0.6	3.2 ± 1.1	2.7 ± 1.0	4.7 ± 1.9	4.0 ± 1.6	8.3 ± 7.3	7.2 ± 2.9	7.6 ± 3.3	5.6 ± 2.6
FFA	22.9 ± 5.6	21.1 ± 3.0	20.0 ± 3.4	23.4 ± 4.0	25.6 ± 4.6	33.3 ± 11.9	26.0 ± 3.7	26.9 ± 2.7	26.1 ± 3.4
CE	1.4 ± 0.5	1.3 ± 0.3	1.3 ± 0.3	1.9 ± 0.5	2.2 ± 0.6	6.3 ± 1.6	10.7 ± 4.7	12.7 ± 5.0	13.4 ± 3.2
Phospholipids									
PC	15.5 ± 1.3	15.7 ± 1.2	14.8 ± 1.0	15.4 ± 0.7	14.7 ± 2.3	14.3 ± 1.4	13.8 ± 2.1	12.6 ± 1.0	12.1 ± 1.2
PE	9.6 ± 2.1	9.5 ± 1.6	8.9 ± 1.6	8.7 ± 1.0	9.3 ± 2.1	8.2 ± 1.9	7.2 ± 2.3	6.4 ± 0.9	5.6 ± 1.3
LPC	2.9 ± 0.9	2.6 ± 0.9	2.5 ± 1.2	2.1 ± 0.5	2.8 ± 0.7	2.6 ± 0.7	2.2 ± 0.6	1.7 ± 0.4	2.0 ± 0.5
LPE	0.9 ± 0.4	0.8 ± 0.6	0.7 ± 0.4	0.5 ± 0.2	0.9 ± 0.4	0.7 ± 0.3	0.5 ± 0.2	0.4 ± 0.2	0.5 ± 0.2
SM	9.5 ± 1.3	8.9 ± 1.6	8.5 ± 2.3	7.7 ± 1.2	7.6 ± 1.6	6.3 ± 0.8	5.3 ± 1.0	4.3 ± 0.8	4.5 ± 0.7
CER	0.5 ± 0.0	0.5 ± 0.1	0.6 ± 0.3	0.4 ± 0.1	0.5 ± 0.1	0.4 ± 0.1	0.4 ± 0.1	0.5 ± 0.1	0.5 ± 0.1
DCER	0.028 ± 0.003	0.031 ± 0.005	0.040 ± 0.022	0.024 ± 0.004	0.031 ± 0.008	0.029 ± 0.006	0.027 ± 0.006	0.024 ± 0.006	0.027 ± 0.005
HCER	0.035 ± 0.003	0.030 ± 0.003	0.030 ± 0.007	0.032 ± 0.004	0.036 ± 0.008	0.042 ± 0.008	0.045 ± 0.007	0.045 ± 0.006	0.050 ± 0.006
LCER	0.005 ± 0.001	0.004 ± 0.002	0.005 ± 0.002	0.004 ± 0.002	0.005 ± 0.002	0.005 ± 0.002	0.008 ± 0.003	0.008 ± 0.002	0.008 ± 0.002

Lipid class concentrations in nmol/mg liver. TAG = Triacylglycerols, DAG = Diacylglycerols, FFA = free fatty acids, CE = Cholesterol esters, PC = Phosphatidylcholines, PE = Phosphatidylethanolamines, LPC = Lysophosphatidylcholines, LPE = Lysophosphatidylethanolamines, SM = Sphingomyelins, CER = Ceramides, DCER = Dihydroceramides, HCER = Hexosylceramides, LCER = lactosylceramide. Data represents mean ± SD with significant differences between HFD and chow per time point ($p < 0.05$) were indicated in the HFD-fed groups, with significant increases shown in red and significant decreases shown in green.

Table 4
Upstream regulators involved in lipid metabolism.

	HFD vs chow	
Upstream regulator	***Z-score***	***p-value***
PPARGC1A	-4.7	0.000
PPARGC1B	-2.3	0.064
ESRRA	-0.9	0.000
NRF1	-1.0	0.027
CLUH	-1.9	0.000
AMPK	-1.8	0.017
SIRT1	-3.7	0.000
UCP1	-1.4	0.000
PPARA	-0.8	0.000
ACOX1	-5.6	0.000
SREBF1	1.4	0.000
PRKCD	4.2	0.059
PRKCE	0.7	0.001
SOD1	-1.7	0.000
SOD2	-0.2	0.000
CAT	-2.2	0.000
GPX1	-1.2	0.000
GR	-2.4	0.000

Upstream regulator analysis used gene expression data after 38 weeks of diet to predict the activity of an upstream regulator unrelated to its expression on protein level. The analysis integrates changes in the expression of all known target genes downstream from a particular regulator. The predicted activity of an upstream regulator is represented by a Z-score, a negative Z-score indicates inhibition of the respective regulator (shown in green), and a positive Z-score indicates activation (shown in red). The p-value < 0.05 in grey indicates significant enrichment of the genes downstream of a regulator, i.e., that more downstream genes are affected than can be expected by chance. N/A indicates an insufficient number of differentially expressed genes to predict the activation state of an upstream regulator.

immunoreactivity inside hepatocytes after 12 weeks, especially in the pericentral area in hypertrophic hepatocytes and those containing microvesicular steatosis (representative images in Fig. 3A). The latter is associated with mitochondrial dysfunction and oxidative stress [44,45], and these observations are consistent with the view that oxidative stress leads to 4-HNE formation prior to cell death and inflammation. In addition to this intrahepatocellular immunoreactivity, 4-HNE positivity was also observed in immune cell clusters and crown-like structures. Quantification of these structures demonstrated that 4-HNE immunoreactivity was practically absent in chow, whereas HFD feeding induced 4-HNE immunoreactivity after 16 weeks progressed up to 38 weeks (Fig. 3B). 4-HNE positive immunoreactivity significantly correlated with microvesicular steatosis, inflammation and hepatic collagen content (Supplemental Fig. S3).

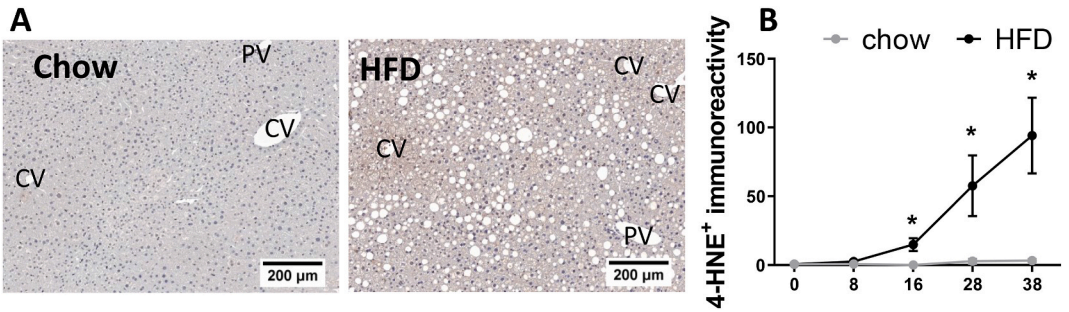

Fig. 3. Hepatic oxidative stress induced lipid peroxidation. (**A**) Illustrative pictures of 4-HNE with indications for the central veins (CV) and portal veins (PV). (**B**) 4-HNE quantification. The x-axis indicates the time in weeks and data are presented as mean ± SEM. * $p < 0.05$ compared to the chow control group.

In line with these histological observations, the upstream regulator analysis of hepatic gene expression predicted that HFD feeding reduced the activity of anti-oxidant enzymes catalase (CAT), Glutathione peroxidase 1 (GPX1), superoxide dismutase 1 (SOD1) and glutathione reductase (GR) (Table 4). In addition, NGS pathway analysis demonstrated that the biological pathway 'mitochondrial dysfunction' was significantly affected in HFD animals.

Taken together, after 8 weeks HFD feeding increased intrahepatic concentrations of specific bioactive lipids such as FFAs, CE and DAGs as well as the oxidative stress marker 4-HNE. Specifically, the early observed 4-HNE immunoreactivity in (enlarged) hepatocytes is indicative of metabolic dysfunction in NAFLD development, while the 4-HNE immunoreactivity associated with inflammatory cells and CLS is indicative of either clearance of 4-HNE positive debris by immune cells, or the formation of ROS and lipid oxidation products by immune cells themselves.

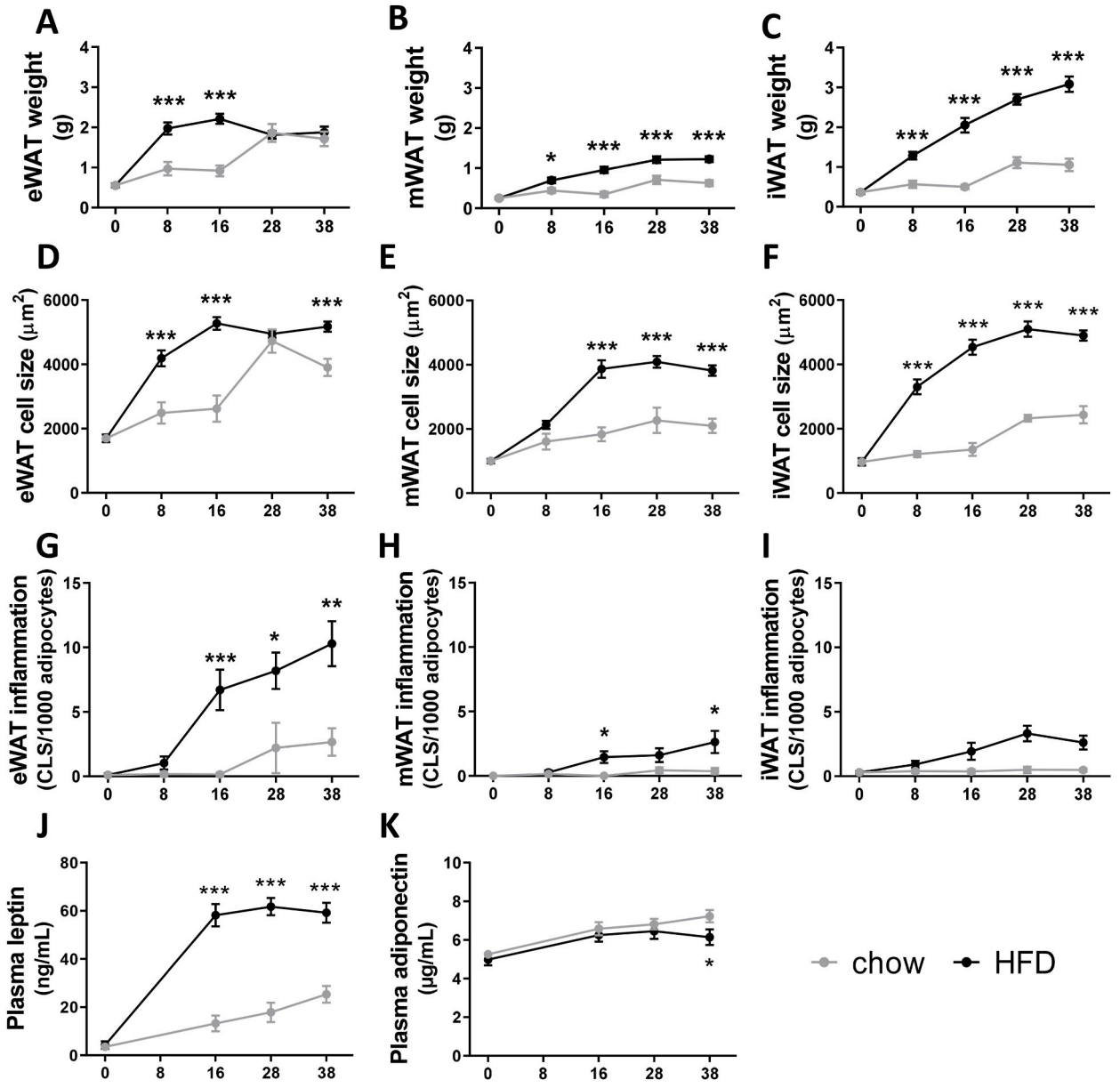

Fig. 4. Obesity-associated white adipose tissue dysfunction during NAFLD development. Adiposity scored in visceral (**A**) epididymal white adipose tissue (eWAT) weight, (**B**) mesenteric WAT (mWAT), and subcutaneous (**C**) inguinal WAT (iWAT). Cell morphometry analysis to determine average cell sizes of (**D**) eWAT, (**E**) mWAT and (**F**) iWAT. The number of crown-like structures (CLS) per 1000 adipocytes was scored to determine (**G**) eWAT inflammation, (**H**) mWAT inflammation and (**I**) iWAT inflammation. Circulating adipokine concentrations were determined in 5h-fasted plasma, including (**J**) leptin and (**K**) adiponectin. The x-axis indicates the time in weeks and data are presented as mean ± SEM. * $p < 0.05$, ** $p < 0.01$, *** $p < 0.001$ compared to the chow control group.

3.4. Visceral white adipose tissue dysfunction but not subcutaneous white adipose tissue dysfunction precedes the development of NASH and liver fibrosis

To determine whether adipose tissue (dys)function might contribute to liver disease development, histological analyses of visceral and subcutaneous WAT depots as well as analysis of circulating adipokines over time was performed. In both chow and HFD-fed mice early body fat mass increases were associated with an early expansion of the eWAT, a visceral depot that seemed to reach its maximum expansion capacity after 8 weeks of HFD, while in chow-fed animals it took 28 weeks to reach a similar weight (Fig. 4A). By contrast, the visceral mWAT depot expansion was minimal in both chow and HFD fed mice, although significantly higher with HFD (Fig. 4B). The subcutaneous inguinal white adipose tissue (iWAT) continued to rise in mass and this increase was linear during 38 weeks of HFD resulting in a 3-fold higher weight gain compared to chow (Fig. 4C). These observations are comparable to the changes in average adipocyte cell size, with the strongest increase in cell size in the eWAT depot in both chow and HFD fed animals (Fig. 4D–F).

Adipose tissue inflammation, scored by the number of crown-like structures, was very low in chow-fed animals with incidental CLS apparent after 28 weeks in the eWAT depot while they were almost entirely absent in the mWAT and iWAT depot (Fig. 4G–I). In contrast, HFD increased CLS numbers in eWAT after 8 weeks and this reached significance from 16 weeks onwards. mWAT inflammation was overall much lower than in eWAT, though HFD feeding still significantly increased the number of CLS at 16 and 38 weeks. HFD also slightly increased the number of CLS in subcutaneous iWAT, but this depot did not become significantly inflamed compared to chow (Fig. 4I) which is in line with its presumed role as a safe storage depot.

In line with these data, plasma levels of the pro-inflammatory adipokine leptin only slightly increased with chow, while HFD increased leptin levels early with tripled concentrations after 16 weeks after which they remained high (Fig. 4J). Plasma levels of the anti-inflammatory adipokine adiponectin remained comparable in chow and HFD mice until 28 weeks, after which adiponectin continued to rise in chow but significantly declined in HFD fed mice (Fig. 4K).

These data indicate that the time point of maximal eWAT expansion coincides with the development of CLS in adipose tissue. Hypertrophy in mWAT and sWAT is a much slower process and these depots do not appear to reach maximal expansion within the period studied. These depots start to become inflamed once NASH is established. Therefore, it is possible that circulating factors that

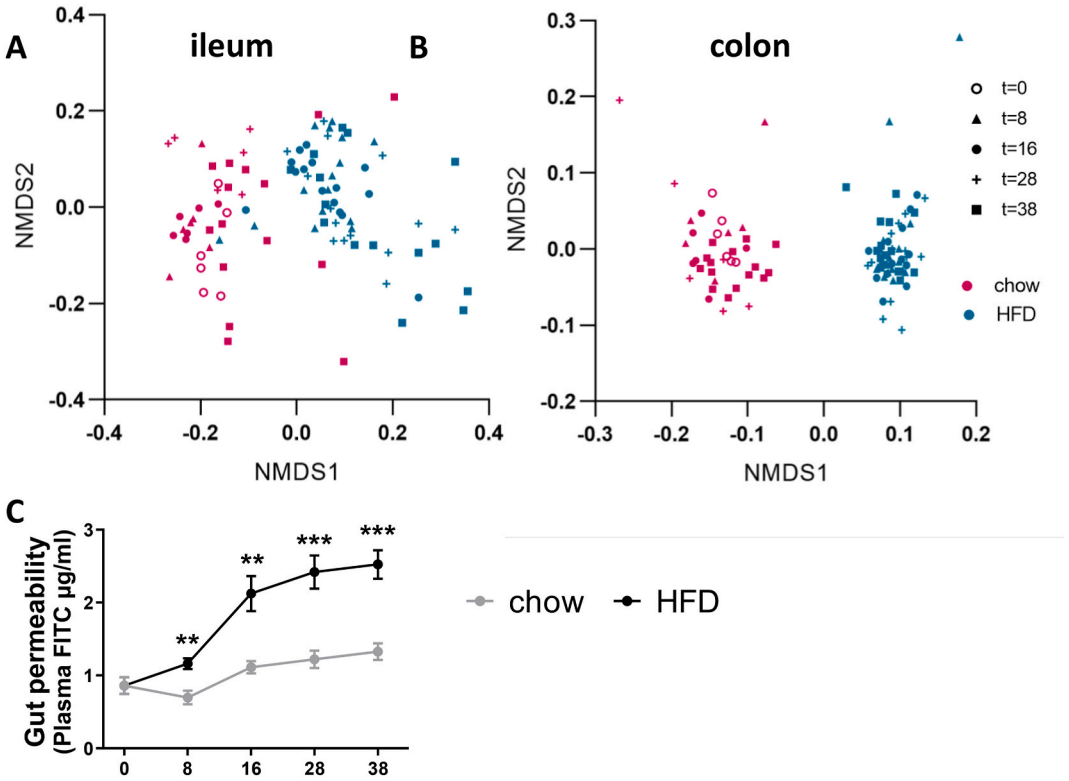

Fig. 5. Gut dysbiosis, increased gut permeability and altered circulating microbiota derived metabolites during NAFLD development. Microbiota composition was studied using 16s rRNA gene analysis in the mucosal compartments of both the ileum and colon over time. The microbiota composition was visualized by non-metric multidimensional scaling (NMDS), using the Bray–Curtis index, of the (**A**) the ileum and (**B**) colon: every dot represents the microbiota composition of one mouse and the distance between dots represents how (dis)similar the microbiota composition is between these mice. (**C**) Functional gut permeability was determined using fluorescent labelled dextran's (FD4 test). The x-axis represents the time in weeks and data are presented as mean ± SEM. * $p < 0,05$, ** $p < 0,01$, *** $p < 0,001$ compared to the chow control group.

may affect NAFLD progression are mainly derived from an early hypertrophic inflamed visceral eWAT depot, although it cannot be excluded that lipids draining from the mesenteric depot into the liver also contribute to the lipid load during the course of disease.

3.5. *Increased gut permeability and microbiota dysbiosis associated with altered plasma bile acid and SCFA concentrations precede the development of NASH and liver fibrosis*

To investigate gut dysfunction during NASH development, microbiota composition, gut permeability and circulating gut-derived metabolites (SCFAs and bile acids) were analyzed.

Mucosal microbiota composition changes were analyzed with 16sRNA in the mucosa of the ileum and colon and are visualized by non-metric multidimensional scaling (NMDS) (Fig. 5). Every dot in this NDMS graph represents the total microbiota composition of one mouse and close distances between dots represent similarity in microbiota composition. All mice were on a chow diet at t = 0 indicated by the black circle in the ileum and colon, over time the chow-fed mice remained clustered together with more diverse compositions in the ileum compared with the colon compartment. In contrast, HFD feeding induced a pronounced shift in microbiota composition within 8 weeks. Thereafter, HFD-fed mice continued to overlap in both the ileum (Fig. 5A) and colon compartment (Fig. 5B). Over time HFD feeding continued to significantly increase the abundance of genera including for instance *Allobaculum, Clostridium_IV* and *Clostridium_XI*. A complete overview of time-resolved changes in microbiota abundance in both compartments during NAFLD progression is provided in Supplemental Fig. S4. Statistical analysis of microbiota compositions using permutation tests confirmed that the microbiota composition of HFD-fed mice was significantly altered from 8 weeks onwards.

Gut permeability was assessed by the ability of FITC-labelled dextran to pass from the intestinal lumen into the circulation, which is thought to reflect paracellular permeability (FD4 test) (Fig. 5C). Gut permeability in chow-fed animals remained low and stable over time, whereas HFD feeding significantly increased gut permeability already after 8 weeks and continued to increase over time.

To investigate whether the gut microbiota and gut permeability changes associated with alterations in circulating levels of gut-derived metabolites, we analyzed the levels of SCFAs and bile acids in fasting plasma. Total plasma SCFA concentrations were not affected during HFD-induced NASH development (Supplemental Fig. S5A), but the SCFA composition did shift with HFD feeding (Table 5). Specifically, a rise in the less abundant SCFA caproate, isobutyrate, methylbutyrate, valerate and isovalerate were observed. Circulating total bile acids in chow-fed mice decreased over time while in HFD-fed mice they increased towards the end of the study (Supplemental Fig. S5B). After 38 weeks of HFD total bile acids were significantly elevated compared to chow (Table 6), including specific bile acids G-CA, T-CA, DCA, T-CDCA and T-UDCA that were reportedly elevated in NASH patients (underlined in Table 6) [46].

In conclusion, the observed early increase in gut permeability is in line with the significant change in microbiota composition as well as changes in circulating gut-derived metabolites involved in organ crosstalk. Gut dysfunction including microbiota dysbiosis, increased gut permeability and altered gut-derived metabolites precede hepatic inflammation and fibrosis.

Table 5
Circulating short-chain fatty acid (SCFA) concentrations as gut-liver crosstalk mediator.

	Chow					HFD			
	T=0	T=8	T=16	T=28	T=38	T=8	T=16	T=28	T=38
Acetate	2.556 ± 0.797	4.098 ± 1.522	3.832 ± 2.019	2.866 ± 0.676	3.423 ± 1.117	5.383 ± 1.997	3.456 ± 1.034	2.726 ± 0.818	3.392 ± 0.544
Butyrate	0.083 ± 0.053	0.086 ± 0.041	0.082 ± 0.029	0.043 ± 0.019	0.050 ± 0.023	0.060 ± 0.025	0.056 ± 0.030	0.049 ± 0.017	0.048 ± 0.019
Caproate	0.075 ± 0.017	0.101 ± 0.032	0.103 ± 0.032	0.092 ± 0.025	0.091 ± 0.025	0.191 ± 0.092	0.205 ± 0.082	0.307 ± 0.126	0.164 ± 0.074
Isobutyrate	0.025 ± 0.012	0.024 ± 0.007	0.038 ± 0.009	0.027 ± 0.008	0.024 ± 0.012	0.028 ± 0.008	0.033 ± 0.013	0.043 ± 0.015	0.028 ± 0.006
Methylbutyrate	0.027 ± 0.006	0.032 ± 0.010	0.043 ± 0.007	0.033 ± 0.008	0.024 ± 0.004	0.030 ± 0.010	0.041 ± 0.013	0.050 ± 0.015	0.033 ± 0.008
Valerate	0.003 ± 0.005	0.005 ± 0.003	0.006 ± 0.002	0.006 ± 0.003	0.001 ± 0.001	0.006 ± 0.003	0.009 ± 0.007	0.013 ± 0.005	0.007 ± 0.003
Isovalerate	0.011 ± 0.002	0.010 ± 0.035	0.013 ± 0.004	0.011 ± 0.004	0.014 ± 0.006	0.019 ± 0.008	0.020 ± 0.008	0.027 ± 0.010	0.020 ± 0.008

Fasted plasma SCFA concentrations in μg/ml. Data represent mean ± SD with significant differences between HFD and chow per time point ($p < 0.05$) were indicated in the HFD-fed groups, with significant increases shown in red.

Table 6
Circulating bile acid concentrations as gut-liver crosstalk mediator.

	Chow					HFD			
	T=0	T=8	T=16	T=28	T=38	T=8	T=16	T=28	T=38
Primary BA									
Cholic acid (CA)	0.638 ± 0.312	0.496 ± 0.141	0.433 ± 0.251	0.388 ± 0.358	0.280 ± 0.164	0.061 ± 0.050	0.124 ± 0.097	0.252 ± 0.168	0.295 ± 0.241
Taurocholic acid (T-CA)	0.167 ± 0.082	0.255 ± 0.116	0.139 ± 0.070	0.203 ± 0.246	0.202 ± 0.184	0.343 ± 0.406	0.743 ± 1.108	1.589 ± 1.823	1.692 ± 1.569
Glycocholic acid (G-CA)	0.005 ± 0.003	0.005 ± 0.002	0.003 ± 0.002	0.003 ± 0.001	0.003 ± 0.002	0.002 ± 0.001	0.004 ± 0.004	0.010 ± 0.011	0.011 ± 0.010
Chenodeoxycholic acid (CDCA)	0.022 ± 0.003	0.018 ± 0.002	0.017 ± 0.013	0.014 ± 0.021	0.011 ± 0.007	0.001 ± 0.003	0.007 ± 0.009	0.013 ± 0.009	0.012 ± 0.005
Taurochenodeoxycholic acid (T-CDCA)	0.005 ± 0.002	0.011 ± 0.005	0.005 ± 0.001	0.007 ± 0.008	0.009 ± 0.007	0.020 ± 0.012	0.038 ± 0.045	0.077 ± 0.061	0.074 ± 0.042
Secondary BA									
Deoxycholic acid (DCA)	1.223 ± 0.185	0.305 ± 0.192	0.729 ± 0.150	0.292 ± 0.216	0.377 ± 0.155	0.263 ± 0.163	0.487 ± 0.205	0.525 ± 0.228	0.527 ± 0.212
Taurodeoxycholic acid (T-DCA)	0.096 ± 0.020	0.082 ± 0.066	0.069 ± 0.011	0.034 ± 0.015	0.055 ± 0.042	0.184 ± 0.131	0.206 ± 0.151	0.319 ± 0.314	0.203 ± 0.092
Ursodeoxycholic acid (UDCA)	0.081 ± 0.016	0.098 ± 0.016	0.102 ± 0.040	0.045 ± 0.039	0.056 ± 0.035	0.008 ± 0.010	0.042 ± 0.021	0.035 ± 0.021	0.044 ± 0.028
Tauro-ursodeoxycholic acid (T-UDCA)	0.030 ± 0.020	0.021 ± 0.004	0.015 ± 0.004	0.015 ± 0.010	0.018 ± 0.009	0.048 ± 0.022	0.063 ± 0.055	0.098 ± 0.068	0.100 ± 0.056

Fasted plasma bile acid concentrations in μM. Data represent mean ± SD with significant differences between HFD and chow per time point ($p < 0.05$) were indicated in the HFD-fed groups, with significant increases shown in red and significant decreases shown in green.

4. Discussion

In the current study we extensively characterized the sequence of pathogenic events during NAFLD development in multiple organs (liver, gut, adipose tissue) as well as circulating metabolites implicated in organ crosstalk. Ldlr−/−.Leiden mice on a HFD develop obesity, plasma dyslipidemia (e.g., increased cholesterol and triglycerides, mainly confined to the atherogenic apo-B containing lipoproteins) and insulin resistance, as observed in NASH patients. In this translational context we observed that WAT dysfunction (specifically eWAT inflammation) and gut dysfunction (microbiota dysbiosis, increased gut permeability, and altered composition of gut-derived metabolites) precede the development of NASH and liver fibrosis. In the liver, early metabolic dysfunction manifests as an increase in lipid accumulation (steatosis), mainly in the form of triglycerides but also FFA, cholesterol esters and low abundant bioactive lipids such as DAGs. Intrahepatic hits from free cholesterol, FFA and oxidative stress-induced 4-HNE can promote hepatic inflammation and fibrosis.

In humans, NAFLD develops over decades, with obesity and insulin resistance as the main risk factors for progression [1]. Likewise, diet-induced liver disease progression is relatively slow in mouse models that use translational experimental set-ups to mimic human pathophysiology (e.g., using diets that have human-like macronutrient composition), such as reported herein for the Ldlr−/−.Leiden model. Other NASH models using experimental diets that contain high concentrations of cholesterol up to 1% or even 2% (w/w of diet) may develop liver pathology faster, however this is at the cost of translational value. Treatment with exogenous dietary cholesterol increases intrahepatic free cholesterol, but shuts down endogenous cholesterol synthesis in the liver [47–49]. The excess cholesterol in these models is the single driver of the NASH pathology (i.e. it is required for disease induction) [50]. In contrast, increased intrahepatic free cholesterol in NASH patients is due to endogenous increase in hepatic cholesterol synthesis and is one of many pathways involved in the complex multi-organ disease progression of NAFLD (these intrahepatic free cholesterol concentrations in NASH patients are reflected in the Ldlr−/−.Leiden mouse [17]). Another frequently-used NASH model is based on the restriction of dietary choline and methionine, which leads to impairment in the assembly and secretion of VLDL particles by the liver. Intrinsic to this strategy to experimentally induce steatosis, these models lack dyslipidemia and are normolipidemic, and are characterized by severe body weight loss which contrasts NASH patients. Of note, although dietary methionine and choline deficiency is not translational to NASH patients, these mouse models may be relevant for a specific subset of NASH patients that have impaired VLDL secretion [16].

In Ldlr−/−.Leiden mice, HFD-feeding induced a pronounced increase in plasma cholesterol and TAGs mainly confined in the

atherogenic apoB-containing (V)LDL lipoprotein particles. This reduced clearance of apoB-containing lipoprotein particles in the Ldlr−/−.Leiden model is akin to the human situation and results in similar lipoprotein profiles as observed in subjects with NASH [51]. In addition, the HFD-induced increases in (V)LDL in the Ldlr−/−.Leiden mouse are accompanied by a pronounced increase in oxLDL [52]. The genetic alteration of the LDL receptor in this model is not the driver of NAFLD/NASH development (which is induced by HFD feeding in the model, not by the genetic alteration in itself), but rather it is a tool to establish a lipid environment in the liver and plasma compartment that mimics the human situation, with vascular complications that affect vessels and capillaries in- and outside the liver. A consequent limitation of this genetic alteration is that the Ldlr−/−.Leiden mouse is unsuitable to study the effects therapeutics requiring a functional ldl-receptor. Diet-induced dyslipidemia promotes the development of atherosclerosis, the major underlying cause of cardiovascular disease (CVD) and this is typically also observed in the HFD-treated Ldlr−/−.Leiden model [16,20]. The presence of atherosclerosis in conjunction with NAFLD/NASH is important because cardiovascular disease (CVD) is the major overall cause of mortality in NASH patients. This is also reflected in a head-to-head metabolomics comparison of HFD-treated Ldlr−/−.Leiden mice with n = 1099 NASH patients, demonstrating that a large portion of NASH patients is at risk of CVD disease and the metabolome of these patients corresponds with that of the Ldlr−/−.Leiden mice [16].

Hepatic fat accumulation during NAFLD development was mainly attributable to an increase in triglyceride content in the HFD-fed mice. These triglycerides are considered an inert and safe storage form of energy [53]. At the same time HFD feeding significantly elevated hepatic CE, DAGs and temporarily increased FFA during early NASH development. In line with our data a recent cohort of 365 biopsies ranging from non-steatosis obesity to NASH found that TAGs, DAGs and CE were significantly increased in NASH patients [54]. Specifically, the accumulation of the less abundant lipid species seems detrimental for cell function. In sedentary humans, even in young individuals, DAGs and CER have been shown to directly bind to protein kinase C and block insulin receptor function (5, 6), [55, 56]. Importantly, DAGs were found to correlate best with insulin resistance (compared to for example body mass index and ceramides) [42,57]. This correlation of DAGs and insulin resistance has been confirmed in both mice [53] and humans [58] in clamp experiments specifically examining insulin sensitivity.

The high liver lipid load in NAFLD challenges the peroxisomes and mitochondria to utilize the excess fat. Excessive lipid oxidation gives rise to a chronic increase in reactive oxygen species (ROS) [43,59]. In HFD-fed Ldlr−/−.Leiden mice, we demonstrated that already after 12 weeks of HFD feeding, 4-HNE positive immunoreactivity is observable inside hepatocytes that are often hypertrophic, thus lending support to the notion that they are overloaded by lipids and oxidative stress. In the current study we showed that 4-HNE immunoreactivity continuously increased during NAFLD development, together with a predicted deactivation of anti-oxidant enzymes (CAT, GPX1, SOD1, GSR) after 38 weeks of HFD. This suggests that persistent oxidative stress causes damage to the hepatocyte, consistent with the view that oxidative stress occurs prior to inflammation and cell death and may deplete the anti-oxidant safeguards. Our data is also consistent with findings in NAFLD patients, in which ROS and byproducts of ROS-induced lipid peroxidation are elevated and are associated with disease severity [7,60]. Furthermore, intrahepatic glutathione content and anti-oxidant enzyme activity of SOD and catalase are significantly decreased in NAFLD patients [60,61].

NAFLD progression from lipid accumulation to hepatic inflammation together with increases in 4-HNE immunoreactivity are potentially directly linked. Many examples of this link exist: 1) activation of TLR4 by saturated FFA [62] 2) accumulation of intrahepatic cholesterol and subsequent formation of cholesterol crystals which activate the NLP3 inflammasome [63] 3) formation of 4-HNE which can bind and activate the inflammatory receptor SRC, thereby activating NF-kB signaling [64]. Conversely, inflammation may also stimulate hepatic lipid accumulation: TKB1, activated by pro-inflammatory stimuli, has been shown to repress energy expenditure by phosphorylating and inhibiting the key metabolic regulator AMPK [65]. Although beyond the scope of the current study, the muscle may also affect the inflammatory status of the liver as exercise improved muscle health in HFD fed Ldlr−/−.Leiden mice and associated with improvements in hepatic inflammation [3]. The activation of local macrophages and their shift towards a proinflammatory phenotype promotes the secretion of cytokines and chemokines to recruit monocytes and neutrophils to the liver and amplify the inflammatory response. Indeed, 8 weeks of HFD resulted in an increase in cytokine IL-17 and chemokines MIP1a (CCL3), RANTES (CCL5), KC (CXCL1), IP-10 (CXCL10), all of which are critical for immune cell infiltration and also observed in human livers. The rise in intrahepatic cytokines and chemokines resulted in mixed inflammatory infiltrates in the liver as observed in HE sections and by increased F4/80 positive CLS, essentially as observed in NASH patients [8].

It is thought that persistent hepatocellular damage and inflammation are drivers of fibrosis, which is by itself a key prognostic marker of all-cause mortality in NAFLD patients [66]. The signals that can activate hepatic stellate cells, the main producers of extracellular matrix proteins including collagens, are manifold [67]. These include cytokines such as TGF-β but also metabolites such as 4-HNE from oxidative stress-induced lipid peroxidation. The observed early increases in leptin from adipose tissue can also directly stimulate hepatic stellate cell activation [68,69]. These extrahepatic signals such as leptin that can promote fibrosis in the liver suggest that treatment for NAFLD should not be limited to the liver but should also correct dysmetabolic states in distant organs with metabolic crosstalk to the liver.

Adipose tissue hypertrophy and inflammation, particularly in the eWAT depot, preceded evident NASH development in the current study. During diet-induced metabolic overload WAT depots can expand by adipocyte hyperplasia (an increase in cell number via adipogenesis) and adipocyte hypertrophy (an increase in cell size). Both processes are thought to have physiological limits, and in this study we demonstrate that these vary between different WAT depots, as was also observed in C57BL/6J mice fed the same HFD [70]. In this study, we have shown that the time point of maximal eWAT expansion coincides with the development of CLS in adipose tissue indicating that processes occurring at maximal hypertrophy form triggers for immune cell infiltration and cellular inflammation. This is supported by the observation that particularly the large (hypertrophic) adipocytes are the main source of inflammatory mediators while smaller adipocytes hardly release inflammatory factors in *ex vivo* cultured adipocytes from obese men [71]. Hypertrophic inflamed eWAT in Ldlr−/−.Leiden mice is associated with predicted activation of inflammatory upstream regulators including

cytokines and chemokines [3,22] as well as increases in circulating levels of SAA, E-selectin and TNFα [3]. The development of adipocyte hypertrophy in mWAT and sWAT is a slower process, and these depots became inflamed when NASH is already histologically manifest. Therefore, it is likely that circulating factors that may affect NASH development in mice are mainly derived from an early hypertrophic inflamed eWAT depot. Consistent with this observation, we also demonstrated that the surgical removal of inflamed eWAT in C57BL/6J mice on a HFD resulted in a significant reduction in NASH [70]. The visceral adipose tissue in humans is also considered to be the most detrimental and visceral obesity is associated with a predisposition for developing disorders including insulin resistance, CVD and NAFLD, while storing fat in the subcutaneous depot is considered a more safe way and does not associate with insulin resistance [72]. This is further supported by higher cytokine secretion by cultured visceral derived adipocytes compared with subcutaneous adipocytes [73]. Subcutaneous adipocytes on the other hand, secrete more adiponectin and may therefore be more beneficial [73]. A potential link between NAFLD and dysfunctional WAT is an elevated lipolysis in these depots as they become insulin resistant. Impaired insulin action can increase the flux of FFA towards the liver. This notion is further supported by the fact that the degree of insulin resistance in adipose tissue is tightly associated with NAFLD severity [74]. Of note, the FFA influx has been shown to account for 60% of TAG in livers of NAFLD patients, while only 25% of the TAGs is derived from DNL and 15% from the diet [75].

In this study, HFD feeding induced an early shift in microbiota composition, altered circulating microbiota derived metabolite concentrations BA and SCFA and increased gut permeability before NASH developed. Therefore it seems likely that the gut could play a role in NAFLD development, consistent with reports of mice without gut microbiota that were resistant to diet-induced obesity, liver steatosis and insulin resistance [76,77]. The microbiota regulates bile acid homeostasis [78], is involved in metabolic processes such as glucose, lipid and energy homeostasis [79], and it produces (via fermentation of carbohydrates and proteins) short chain fatty acids (SCFAs) [80,81]. After the major shift in microbiota composition at t = 8w, we observed only minor changes in microbiota composition during NAFLD progression. Nonetheless, It is possible that changes in microbiota function (i.e. diet processing and metabolite production) may have changed over time and in that respect were able to affect NASH progression. This notion is in line with our observations that circulating levels of microbiota-derived metabolites (SCFA, BCFA, secondary bile acids) change over time throughout the study. These microbiota-derived metabolites may impact NAFLD/NASH progression because they have roles in energy metabolism and can modulate inflammation [25,34]. Nonetheless, the extent to which these changes over time contribute to experimental NASH/fibrosis development cannot be determined based on the currently available data. Interestingly, the increase in total circulating bile acids of T-CA, G-CA, T-CDCA, DCA and T-UDCA with HFD, were also reported to be elevated in plasma of NASH patients [46]. Fecal transplantation of microbiota from healthy lean subjects into NAFLD patients improved intestinal permeability, confirming that microbiota composition and gut barrier function are linked [82]. Similarly, it was demonstrated that fecal transplantation had beneficial effects on liver markers including gamma-glutamyl transferase and tended to improve ALT which also suggest a link between gut and the liver. Indeed increases in intestinal permeability have also been shown to correlate with liver disease severity [83]. In a recent study, we increased Bifidobacterium and transiently improved gut permeability (FD4 test) using the prebiotic 2′-fucosyllactose. This improvement of dysbiosis and gut permeability was accompanied by lower LPS binding protein levels, reduced liver steatosis and reductions in DAGs, further supporting the role of the gut and its microbiota in the control of metabolic homeostasis [24].

Intrinsic to the setup of the study we cannot demonstrate causation of metabolic dysfunction in the liver or dysfunctional WAT or gut/microbiota during the development of NAFLD. The potential role of metabolic dysfunctions in these organs in NAFLD development have been reported previously using interventions that targeted the white adipose tissue [70,84], the gut [24,85], the liver [17,29,86], or multiple organs simultaneously [3,22,25,26,34]. However, this study does provide insight into the temporal dynamics and chronology of these processes and how they interact with each other during the development NAFLD. It is obvious that only processes that proceed a particular biochemical or histological hallmark in liver can contribute to the initiation of this disease hallmark. Nonetheless, we cannot exclude that processes that occur at a relatively late time point in the pathogenesis may still further aggravate the disease from the time point of their occurrence. For instance, changes to the overall anatomical architecture of the liver as demonstrated by Micro-CT may affect the flow properties of the organ at a relatively late stage and thereby may impair both nutrient and oxygen supply as well as hamper bile secretion which will aggravate the pathogenesis.

In conclusion, Ldlr−/−.Leiden mice fed a HFD develop obesity, dyslipidemia and insulin resistance, and the underlying processes involve molecular changes in visceral depots and the gut, dyslipidemia with increased atherogenic apoB-containing lipoproteins, and lipid-induced insulin resistance, essentially as observed in obese NASH patients. These obesity-associated NAFLD features (including a humanized lipid profile and translational dietary conditions) in the Ldlr−/−.Leiden mouse model are comparable to NASH patients, which emphasizes the translational value of the mouse model. In this NAFLD/NASH model we provide temporal insight into the dynamic metabolic dysfunctions underlying NAFLD in the liver, visceral (eWAT and mWAT) and subcutaneous WAT (iWAT) depots and the gut (microbiota). In the liver, metabolic dysfunction manifests as an early accumulation of specific bioactive lipids (DAGs and CER) which can directly promote insulin resistance. This experimental condition is relevant for the study of treatments because additional hits from intrahepatic free cholesterol, FFA and oxidative stress-induced 4-HNE can promote hepatic inflammation and fibrosis. In addition to these intrahepatic triggers, the experimental conditions employed herein also take into account the role of distant organs with metabolic-inflammatory cross-talk to the liver. For instance, epididymal WAT inflammation and gut dysfunction (microbiota dysbiosis and gut permeability) preceded the development of NASH and liver fibrosis and appeared to contribute to NAFLD/NASH on basis of aforementioned published studies. Hence, new strategies aiming at prevention, or attenuation of NAFLD/NASH development should not be limited to the liver but also should consider correcting dysmetabolism and inflammation in other organs that affect metabolic homeostasis in the liver.

Author contribution statement

Eveline Gart: Conceived and designed the experiments; Performed the experiments; Analyzed and interpreted the data; Wrote the paper.

Wim van Duyvenvoorde; Jessic Snabel; Christa de Ruiter; Joline Attema: Performed the experiments;

Martien P.M. Caspers: Contributed reagents, materials, analysis tools or data; Analyzed and interpreted the data.

Serene Lek: Contributed reagents, materials, analysis tools or data; Analyzed and interpreted the data.

Bertie Joan van Heuven: Performed the experiments; Analyzed and interpreted the data.

Arjen Speksnijder; Analyzed and interpreted the data; Contributed reagents, materials, analysis tools or data.

Martin Giera: Performed the experiments; Contributed reagents, materials, analysis tools or data; Wrote the paper.

Aswin Menke: Analyzed and interpreted the data; Wrote the paper.

Kanita Salic: Conceived and designed the experiments.

Kendra K. Bence; Gregory J Tesz: Analyzed and interpreted the data; Wrote the paper.

Jaap Keijer: Analyzed and interpreted the data; Wrote the paper.

Robert Kleemann: Conceived and designed the experiments; Analyzed and interpreted the data; Wrote the paper.

Martine Morrison: Conceived and designed the experiments; Analyzed and interpreted the data; Wrote the paper.

Funding statement

This study was performed within the public-private partnership (PPP) ProLiver, a collaboration project that is co-funded by a PPP Allowance made available by Health~Holland, Top Sector Life Sciences & Health, to stimulate public-private partnerships. The work described here was also supported by the TNO Research Programs Food and Nutrition, and Biomedical Health (PMC 9 and PMC13).

Data availability statement

Data associated with this study has been deposited at GEO under the accession number GSE209762.

Declaration of interest's statement

The authors declare that they have no known competing financial interests or personal relationships that could have appeared to influence the work reported in this paper.

Acknowledgements

We would like to thank Elsbet Pieterman, Nanda Keijzer, Nicole Worms, Anita van Nieuwkoop, Nikki van Trigt, Simone van der Drift and Marijke Voskuilen for their excellent technical assistance. The graphical abstract was created in BioRender.com (2022).

Appendix A. Supplementary data

Supplementary data to this article can be found online at https://doi.org/10.1016/j.heliyon.2023.e13985.

References

[1] R. Loomba, S.L. Friedman, G.I. Shulman, Mechanisms and disease consequences of nonalcoholic fatty liver disease, Cell 184 (2021) 2537–2564, https://doi.org/10.1016/j.cell.2021.04.015.

[2] S.A. Polyzos, E.S. Kang, C. Boutari, E.-J. Rhee, C.S. Mantzoros, Current and emerging pharmacological options for the treatment of nonalcoholic steatohepatitis, Metabolism 111 (2020), 154203, https://doi.org/10.1016/j.metabol.2020.154203.

[3] A.M. van den Hoek, J.C.B.C. de Jong, N. Worms, A. van Nieuwkoop, M. Voskuilen, A.L. Menke, S. Lek, M.P.M. Caspers, L. Verschuren, R. Kleemann, Diet and exercise reduce pre-existing NASH and fibrosis and have additional beneficial effects on the vasculature, adipose tissue and skeletal muscle via organ-crosstalk, Metabolism 124 (2021), 154873, https://doi.org/10.1016/J.METABOL.2021.154873.

[4] D.L. Gorden, P.T. Ivanova, D.S. Myers, J.O. McIntyre, M.N. VanSaun, J.K. Wright, L.M. Matrisian, H.A. Brown, Increased diacylglycerols characterize hepatic lipid changes in progression of human nonalcoholic fatty liver disease; comparison to a murine model, PLoS One 6 (2011), https://doi.org/10.1371/JOURNAL.PONE.0022775.

[5] K. Lyu, Y. Zhang, D. Zhang, M. Kahn, K.W. ter Horst, M.R.S. Rodrigues, R.C. Gaspar, S.M. Hirabara, P.K. Luukkonen, S. Lee, S. Bhanot, J. Rinehart, N. Blume, M. G. Rasch, M.J. Serlie, J.S. Bogan, G.W. Cline, V.T. Samuel, G.I. Shulman, A membrane-bound diacylglycerol species induces pkcε-mediated hepatic insulin resistance, Cell Metabol. 32 (2020), https://doi.org/10.1016/J.CMET.2020.08.001, 654-664.e5.

[6] F. Magkos, X. Su, D. Bradley, E. Fabbrini, C. Conte, J.C. Eagon, J.E. Varela, E.M. Brunt, B.W. Patterson, S. Klein, Intrahepatic diacylglycerol content is associated with hepatic insulin resistance in obese subjects, Gastroenterology 142 (2012), https://doi.org/10.1053/J.GASTRO.2012.03.003, 1444-1446.e2.

[7] C. Koliaki, J. Szendroedi, K. Kaul, T. Jelenik, P. Nowotny, F. Jankowiak, C. Herder, M. Carstensen, M. Krausch, W.T. Knoefel, M. Schlensak, M. Roden, Adaptation of hepatic mitochondrial function in humans with non-alcoholic fatty liver is lost in steatohepatitis, Cell Metabol. 21 (2015) 739–746, https://doi.org/10.1016/j.cmet.2015.04.004.

[8] S.H. Ibrahim, P. Hirsova, G.J. Gores, Non-alcoholic steatohepatitis pathogenesis: sublethal hepatocyte injury as a driver of liver inflammation, Gut 67 (2018) 963, https://doi.org/10.1136/GUTJNL-2017-315691.

[9] I.A. Kirpich, L.S. Marsano, C.J. McClain, Gut-liver axis, nutrition, and non-alcoholic fatty liver disease, Clin. Biochem. 48 (2015) 923–930.

[10] G. Lee, H.J. You, J.S. Bajaj, S.K. Joo, J. Yu, S. Park, H. Kang, J.H. Park, J.H. Kim, D.H. Lee, S. Lee, W. Kim, G.P. Ko, Distinct signatures of gut microbiome and metabolites associated with significant fibrosis in non-obese NAFLD, Nat. Commun. 11 (2020), https://doi.org/10.1038/S41467-020-18754-5.

[11] J. Luther, J.J. Garber, H. Khalili, M. Dave, S.S. Bale, R. Jindal, D.L. Motola, S. Luther, S. Bohr, S.W. Jeoung, V. Deshpande, G. Singh, J.R. Turner, M.L. Yarmush, R.T. Chung, S.J. Patel, Hepatic injury in nonalcoholic steatohepatitis contributes to altered intestinal permeability, Cell Mol. Gastroenterol. Hepatol. 1 (2015) 222, https://doi.org/10.1016/J.JCMGH.2015.01.001.

[12] H. Hu, A. Lin, M. Kong, X. Yao, M. Yin, H. Xia, J. Ma, H. Liu, Intestinal microbiome and NAFLD: molecular insights and therapeutic perspectives, J. Gastroenterol. 55 (2020) 142, https://doi.org/10.1007/S00535-019-01649-8.

[13] M.S. Mirza, Obesity, visceral fat, and NAFLD: queryingthe role of adipokines in the progression of Nonalcoholic fatty liver disease, ISRN Gastroenterol. 2011 (2011) 1–11, https://doi.org/10.5402/2011/592404.

[14] R.S. Taylor, R.J. Taylor, S. Bayliss, H. Hagström, P. Nasr, J.M. Schattenberg, M. Ishigami, H. Toyoda, V. Wai-Sun Wong, N. Peleg, A. Shlomai, G. Sebastiani, Y. Seko, N. Bhala, Z.M. Younossi, Q.M. Anstee, S. McPherson, P.N. Newsome, Association between fibrosis stage and outcomes of patients with nonalcoholic fatty liver disease: a systematic review and meta-analysis, Gastroenterology 158 (2020), https://doi.org/10.1053/J.GASTRO.2020.01.043, 1611-1625.e12.

[15] W. Liang, A.L. Menke, A. Driessen, G.H. Koek, J.H. Lindeman, R. Stoop, L.M. Havekes, R. Kleemann, A.M. Van Den Hoek, Establishment of a general NAFLD scoring system for rodent models and comparison to human liver pathology, PLoS One 9 (2014), https://doi.org/10.1371/journal.pone.0115922.

[16] I. Martínez-Arranz, C. Bruzzone, M. Noureddin, R. Gil-Redondo, I. Mincholé, M. Bizkarguenaga, E. Arretxe, M. Iruarrizaga-Lejarreta, D. Fernández-Ramos, F. Lopitz-Otsoa, R. Mayo, N. Embade, E. Newberry, B. Mittendorf, L. Izquierdo-Sánchez, V. Smid, J. Arnold, P. Iruzubieta, Y.P. Castaño, M. Krawczyk, U. M. Marigorta, M.C. Morrison, R. Kleemann, A. Martín-Duce, L. Hayardeny, L. Vitek, R. Bruha, RA de la Fuente, J. Crespo, M. Romero-Gomez, J.M. Banales, M. Arrese, K. Cusi, E. Bugianesi, S. Klein, S.C. Lu, Q.M. Anstee, O. Millet, N.O. Davidson, C. Alonso, J.M. Mato, Metabolic subtypes of patients with NAFLD exhibit distinctive cardiovascular risk profiles, Hepatology (2022) 1–14, https://doi.org/10.1002/HEP.32427.

[17] M.C. Morrison, L. Verschuren, K. Salic, J. Verheij, A. Menke, P.Y. Wielinga, M. Iruarrizaga-Lejarreta, L. Gole, W. Yu, S. Turner, M.P.M. Caspers, I. Martínez-Arranz, E. Pieterman, R. Stoop, A. van Koppen, A.M. van den Hoek, J.M. Mato, R. Hanemaaijer, C. Alonso, R. Kleemann, Obeticholic acid modulates serum metabolites and gene signatures characteristic of human NASH and attenuates inflammation and fibrosis progression in Ldlr-/-.Leiden mice, Hepatol. Commun. 2 (2018) 1513–1532, https://doi.org/10.1002/hep4.1270.

[18] M.C. Morrison, R. Kleemann, A. van Koppen, R. Hanemaaijer, L. Verschuren, Key inflammatory processes in human NASH are reflected in Ldlr−/−.Leiden mice: a translational gene profiling study, Front. Physiol. 9 (2018), https://doi.org/10.3389/fphys.2018.00132.

[19] A. van Koppen, L. Verschuren, A.M. van den Hoek, J. Verheij, M.C. Morrison, K. Li, H. Nagabukuro, A. Costessi, M.P.M. Caspers, T.J. van den Broek, J. Sagartz, C. Kluft, C. Beysen, C. Emson, A.J. van Gool, R. Goldschmeding, R. Stoop, I. Bobeldijk-Pastorova, S.M. Turner, G. Hanauer, R. Hanemaaijer, Uncovering a predictive molecular signature for the onset of NASH-related fibrosis in a translational NASH mouse model, Cell Mol. Gastroenterol. Hepatol. 5 (2018), https://doi.org/10.1016/j.jcmgh.2017.10.001, 83-98.e10.

[20] A.M. van den Hoek, L. Verschuren, N. Worms, A. van Nieuwkoop, C. de Ruiter, J. Attema, A.L. Menke, M.P.M. Caspers, S. Radhakrishnan, K. Salic, R. Kleemann, A translational mouse model for NASH with advanced fibrosis and atherosclerosis expressing key pathways of human pathology, Cells 9 (2020) 1–21, https://doi.org/10.3390/cells9092014.

[21] E. Gart, E. Souto Lima, F. Schuren, C. de Ruiter, J. Attema, L. Verschuren, J. Keijer, K. Salic, M. Morrison, R. Kleemann, Diet-independent correlations between bacteria and dysfunction of gut, adipose tissue, and liver: a comprehensive microbiota analysis in feces and mucosa of the ileum and colon in obese mice with NAFLD, Int. J. Mol. Sci. 20 (1) (2018), https://doi.org/10.3390/ijms20010001.

[22] E. Gart, K. Salic, M.C. Morrison, M. Caspers, W. van Duyvenvoorde, M. Heijnk, M. Giera, I. Bobeldijk-Pastorova, J. Keijer, A.B. Storsve, P.A. Hals, R. Kleemann, Krill oil treatment increases distinct pufas and oxylipins in adipose tissue and liver and attenuates obesity-associated inflammation via direct and indirect mechanisms, Nutrients 13 (2021), https://doi.org/10.3390/nu13082836.

[23] M.C. Morrison, E. Gart, W. van Duyvenvoorde, J. Snabel, M.J. Nielsen, D.J. Leeming, A. Menke, R. Kleemann, Heat-inactivated akkermansia muciniphila improves gut permeability but does not prevent development of non-alcoholic steatohepatitis in diet-induced obese Ldlr−/−.Leiden mice, Int. J. Mol. Sci. 23 (–17) (2022) 1, https://doi.org/10.3390/ijms23042325.

[24] E. Gart, K. Salic, M.C. Morrison, M. Giera, J. Attema, C. de Ruiter, M. Caspers, F. Schuren, I. Bobeldijk-Pastorova, M. Heer, Y. Qin, R. Kleemann, The human milk oligosaccharide 2′-fucosyllactose alleviates liver steatosis, ER stress and insulin resistance by reducing hepatic diacylglycerols and improved gut permeability in obese Ldlr-/-.Leiden mice, Front. Nutr. 1215 (2022), https://doi.org/10.3389/FNUT.2022.904740.

[25] E. Gart, W van Duyvenvoorde, K. Toet, M.P.M. Caspers, L. Verschuren, M.J. Nielsen, D.J. Leeming, E.S. Lima, A. Menke, R. Hanemaaijer, J. Keijer, K. Salic, R. Kleemann, M.C. Morrison, Butyrate protects against diet-induced NASH and liver fibrosis and suppresses specific non-canonical TGF-β signaling pathways in human hepatic stellate cells, Biomedicines 9 (2021) 1954, https://doi.org/10.3390/BIOMEDICINES9121954.

[26] K. Salic, E. Gart, F. Seidel, L. Verschuren, M. Caspers, W. van Duyvenvoorde, K.E. Wong, J. Keijer, I. Bobeldijk-Pastorova, P.Y. Wielinga, R. Kleemann, Combined treatment with L-carnitine and nicotinamide riboside improves hepatic metabolism and attenuates obesity and liver steatosis, Int. J. Mol. Sci. 20 (2019), https://doi.org/10.3390/IJMS20184359.

[27] E. Gart, W van Duyvenvoorde, M.P.M. Caspers, N van Trigt, J. Snabel, A. Menke, J. Keijer, K. Salic, M.C. Morrison, R. Kleemann, Intervention with isoleucine or valine corrects hyperinsulinemia and reduces intrahepatic diacylglycerols, liver steatosis, and inflammation in Ldlr−/−.Leiden mice with manifest obesity-associated NASH, Faseb. J. 36 (2022), e22435, https://doi.org/10.1096/FJ.202200111R.

[28] M. Ghorasaini, Y. Mohammed, J. Adamski, L. Bettcher, J.A. Bowden, M. Cabruja, K. Contrepois, M. Ellenberger, B. Gajera, M. Haid, D. Hornburg, C. Hunter, C. M. Jones, T. Klein, O. Mayboroda, M. Mirzaian, R. Moaddel, L. Ferrucci, J. Lovett, K. Nazir, M. Pearson, B.K. Ubhi, D. Raftery, F. Riols, R. Sayers, E.J. G. Sijbrands, M.P. Snyder, B. Su, V. Velagapudi, K.J. Williams, Y.B. De Rijke, M. Giera, Cross-laboratory standardization of preclinical lipidomics using differential mobility spectrometry and multiple reaction monitoring, Anal. Chem. 93 (2021) 16369–16378, https://doi.org/10.1021/ACS.ANALCHEM.1C02826.

[29] A.M. Mueller, R. Kleemann, E. Gart, W. van Duyvenvoorde, L. Verschuren, M. Caspers, A. Menke, N. Krömmelbein, K. Salic, Y. Burmeister, B. Seilheimer, M. C. Morrison, Cholesterol accumulation as a driver of hepatic inflammation under translational dietary conditions can Be attenuated by a multicomponent medicine, Front. Endocrinol. (Lausanne) 12 (2021), https://doi.org/10.3389/fendo.2021.601160.

[30] M.I. Love, W. Huber, S. Anders, Moderated estimation of fold change and dispersion for RNA-seq data with DESeq2, Genome Biol. 15 (2014), https://doi.org/10.1186/s13059-014-0550-8.

[31] A. Krämer, J. Green, J. Pollard, S. Tugendreich, Causal analysis approaches in ingenuity pathway analysis, Bioinformatics 30 (2014) 523–530, https://doi.org/10.1093/BIOINFORMATICS/BTT703.

[32] M. Galarraga, J. Campión, A. Muñoz-Barrutia, N. Boqué, H. Moreno, J.A. Martínez, F. Milagro, C. Ortiz-de-Solórzano, Adiposoft: automated software for the analysis of white adipose tissue cellularity in histological sections, J. Lipid Res. 53 (2012) 2791–2796, https://doi.org/10.1194/jlr.D023788.

[33] C.A. Schneider, W.S. Rasband, K.W. Eliceiri, NIH image to ImageJ: 25 years of image analysis, Nat. Methods 9 (2012) 671, https://doi.org/10.1038/NMETH.2089.

[34] A.C. Tengeler, E. Gart, M. Wiesmann, I.A.C. Arnoldussen, W. van Duyvenvoorde, M. Hoogstad, P.J. Dederen, V. Verweij, B. Geenen, T. Kozicz, R. Kleemann, M. C. Morrison, A.J. Kiliaan, Propionic acid and not caproic acid, attenuates nonalcoholic steatohepatitis and improves (cerebro) vascular functions in obese Ldlr-/-.Leiden mice, Faseb. J. (2020) 1–19, https://doi.org/10.1096/fj.202000455R.

[35] T. Liangsupree, E. Multia, J. Metso, M. Jauhiainen, P. Forssén, T. Fornstedt, K. Öörni, A. Podgornik, M.L. Riekkola, Rapid affinity chromatographic isolation method for LDL in human plasma by immobilized chondroitin-6-sulfate and anti-apoB-100 antibody monolithic disks in tandem, Sci. Rep. 91–99 (2019) 1–10, https://doi.org/10.1038/s41598-019-47750-z.

[36] A.J. Kennedy, K.L.J. Ellacott, V.L. King, A.H. Hasty, Mouse models of the metabolic syndrome, Dis Model Mech 3 (2010) 156, https://doi.org/10.1242/DMM.003467.

[37] Q.Q. Zhang, L.G. Lu, Nonalcoholic fatty liver disease: dyslipidemia, risk for cardiovascular complications, and treatment strategy, J. Clin. Transl. Hepatol. 3 (2015) 78, https://doi.org/10.14218/JCTH.2014.00037.

[38] M. Kawanaka, K. Nishino, J. Nakamura, N. Urata, T. Oka, D. Goto, M. Suehiro, H. Kawamoto, G. Yamada, Correlation between serum cytokeratin-18 and the progression or regression of non-alcoholic fatty liver disease, Ann. Hepatol. 14 (2015) 837–844, https://doi.org/10.5604/16652681.1171767.

[39] M.A. Tincopa, Diagnostic and interventional circulating biomarkers in nonalcoholic steatohepatitis, Endocrinol. Diabetes Metab. 3 (2020), e00177, https://doi.org/10.1002/EDM2.177.

[40] M. Itoh, H. Kato, T. Suganami, K. Konuma, Y. Marumoto, S. Terai, H. Sakugawa, S. Kanai, M. Hamaguchi, T. Fukaishi, S. Aoe, K. Akiyoshi, Y. Komohara, M. Takeya, I. Sakaida, Y. Ogawa, Hepatic crown-like structure: a unique histological feature in non-alcoholic steatohepatitis in mice and humans, PLoS One 8 (2013), https://doi.org/10.1371/journal.pone.0082163.

[41] L. Wu, X. Gao, Q. Guo, J. Li, J. Yao, K. Yan, Y. Xu, X. Jiang, D. Ye, J. Guo, The role of neutrophils in innate immunity-driven nonalcoholic steatohepatitis: lessons learned and future promise, Hepatol Int. 14 (2020) 652–666, https://doi.org/10.1007/S12072-020-10081-7/FIGURES/4.

[42] M.C. Petersen, G.I. Shulman, Roles of diacylglycerols and ceramides in hepatic insulin resistance, Trends Pharmacol. Sci. 38 (2017) 649–665.

[43] Z. Chen, R. Tian, Z. She, J. Cai, H. Li, Role of oxidative stress in the pathogenesis of nonalcoholic fatty liver disease, Free Radic. Biol. Med. 152 (2020) 116–141, https://doi.org/10.1016/j.freeradbiomed.2020.02.025.

[44] S.K. Natarajan, C.E. Eapen, A.B. Pullimood, K.A. Balasubramanian, Oxidative stress in experimental liver microvesicular steatosis: role of mitochondria and peroxisomes, J. Gastroenterol. Hepatol. 21 (2006) 1240–1249, https://doi.org/10.1111/j.1440-1746.2006.04313.x.

[45] B. Fromenty, D. Pessayre, Impaired mitochondrial function in microvesicular steatosis effects of drugs, ethanol, hormones and cytokines, J. Hepatol. 26 (1997) 43–53, https://doi.org/10.1016/S0168-8278(97)80496-5.

[46] P. Puri, K. Daita, A. Joyce, F. Mirshahi, P.K. Santhekadur, S. Cazanave, V.A. Luketic, M.S. Siddiqui, S. Boyett, H.K. Min, D.P. Kumar, R. Kohli, H. Zhou, P. B. Hylemon, M.J. Contos, M. Idowu, A.J. Sanyal, The presence and severity of nonalcoholic steatohepatitis is associated with specific changes in circulating bile acids, Hepatology 67 (2018) 534–548, https://doi.org/10.1002/HEP.29359.

[47] P.J.H. Jones, A.S. Pappu, L. Hatcher, Z.C. Li, D.R. Illingworth, W.E. Connor, Dietary cholesterol feeding suppresses human cholesterol synthesis measured by deuterium incorporation and urinary mevalonic acid levels, Arterioscler. Thromb. Vasc. Biol. 16 (1996) 1222–1228, https://doi.org/10.1161/01.ATV.16.10.1222.

[48] J.M. Lecerf, M. De Lorgeril, Dietary cholesterol: from physiology to cardiovascular risk, Br. J. Nutr. 106 (–14) (2011) 6, https://doi.org/10.1017/S0007114511000237.

[49] R. Kleemann, L. Verschuren, M.J. Van Erk, Y. Nikolsky, N.H.P. Cnubben, E.R. Verheij, A.K. Smilde, H.F.J. Hendriks, S. Zadelaar, G.J. Smith, V. Kaznacheev, T. Nikolskaya, A. Melnikov, E. Hurt-Camejo, J. Van der Greef, B. Van Ommen, T. Kooistra, Atherosclerosis and liver inflammation induced by increased dietary cholesterol intake: a combined transcriptomics and metabolomics analysis, Genome Biol. 8 (2007) 1–16, https://doi.org/10.1186/GB-2007-8-9-R200/TABLES/4.

[50] S. Gallage, J.E.B. Avila, P. Ramadori, E. Focaccia, M. Rahbari, A. Ali, N.P. Malek, Q.M. Anstee, M. Heikenwalder, A researcher's guide to preclinical mouse NASH models, Nat. Metab. 4 (2022) 1632–1649, https://doi.org/10.1038/s42255-022-00700-y.

[51] T. Kooistra, L. Verschuren, J. De Vries-Van Der Weij, W. Koenig, K. Toet, H.M.G. Princen, R. Kleemann, Fenofibrate reduces atherogenesis in ApoE*3Leiden mice: evidence for multiple antiatherogenic effects besides lowering plasma cholesterol, Arterioscler. Thromb. Vasc. Biol. 26 (2006) 2322–2330, https://doi.org/10.1161/01.ATV.0000238348.05028.14.

[52] F. Seidel, R. Kleemann, W van Duyvenvoorde, N van Trigt, N. Keijzer, S van der Kooij, C van Kooten, L. Verschuren, A. Menke, A.J. Kiliaan, J. Winter, T. R. Hughes, B.P. Morgan, F. Baas, K. Fluiter, M.C. Morrison, Therapeutic intervention with anti-complement component 5 antibody does not reduce NASH but does attenuate atherosclerosis and MIF concentrations in Ldlr-/-.Leiden mice, Int. J. Mol. Sci. 23 (2022), 10736, https://doi.org/10.3390/IJMS231810736.

[53] M.C. Petersen, G.I. Shulman, Mechanisms of insulin action and insulin resistance, Physiol. Rev. 98 (2018) 2133, https://doi.org/10.1152/PHYSREV.00063.2017.

[54] O. Vvedenskaya, T.D. Rose, O. Knittelfelder, A. Palladini, J.A.H. Wodke, K. Schuhmann, J.M. Ackerman, Y. Wang, C. Has, M. Brosch, V.R. Thangapandi, S. Buch, T. Züllig, J. Hartler, H.C. Köfeler, C. Röcken, Ü. Coskun, E. Klipp, W. Von Schoenfels, J. Gross, C. Schafmayer, J. Hampe, J.K. Pauling, A. Shevchenko, Nonalcoholic fatty liver disease stratification by liver lipidomics, J. Lipid Res. 62 (2021), 100104, https://doi.org/10.1016/J.JLR.2021.100104.

[55] S. Turban, E. Hajduch, Protein kinase C isoforms: mediators of reactive lipid metabolites in the development of insulin resistance, FEBS Lett. 585 (2011) 269–274, https://doi.org/10.1016/J.FEBSLET.2010.12.022.

[56] E. Hajduch, F. Lachkar, P. Ferré, F. Foufelle, Roles of ceramides in non-alcoholic fatty liver disease, J. Clin. Med. 10 (2021) 1–19, https://doi.org/10.3390/JCM10040792.

[57] V.T. Samuel, G.I. Shulman, Mechanisms for insulin resistance: common threads and missing links, Cell 148 (2012) 852–871, https://doi.org/10.1016/j.cell.2012.02.017.

[58] F. Magkos, X. Su, D. Bradley, E. Fabbrini, C. Conte, J.C. Eagon, J.E. Varela, E.M. Brunt, B.W. Patterson, S. Klein, Intrahepatic diacylglycerol content is associated with hepatic insulin resistance in obese subjects, Gastroenterology 142 (2012), https://doi.org/10.1053/J.GASTRO.2012.03.003.

[59] M. Schrader, H.D. Fahimi, Peroxisomes and oxidative stress, Biochim. Biophys. Acta Mol. Cell Res. 1763 (2006) 1755–1766.

[60] Z. Chen, R. Tian, Z. She, J. Cai, H. Li, Role of oxidative stress in the pathogenesis of nonalcoholic fatty liver disease, Free Radic. Biol. Med. 152 (2020) 116–141, https://doi.org/10.1016/J.FREERADBIOMED.2020.02.025.

[61] L.A. Videla, R. Rodrigo, M. Orellana, V. Fernandez, G. Tapia, L. Quiñones, N. Varela, J. Contreras, R. Lazarte, A. Csendes, J. Rojas, F. Maluenda, P. Burdiles, J. C. Diaz, G. Smok, L. Thielemann, J. Poniachik, Oxidative stress-related parameters in the liver of non-alcoholic fatty liver disease patients, Clin. Sci. (Lond.) 106 (2004) 261–268, https://doi.org/10.1042/CS20030285.

[62] A. Georgiadi, S. Kersten, Mechanisms of gene regulation by fatty acids, Adv. Nutr. 3 (2012) 127, https://doi.org/10.3945/AN.111.001602.

[63] E.O. Samstad, N. Niyonzima, S. Nymo, M.H. Aune, L. Ryan, S.S. Bakke, K.T. Lappegård, O.-L. Brekke, J.D. Lambris, J.K. Damås, E. Latz, T.E. Mollnes, T. Espevik, Cholesterol crystals induce complement-dependent inflammasome activation and cytokine release, J. Immunol. 192 (2014) 2837–2845, https://doi.org/10.4049/jimmunol.1302484.

[64] E.J. Jang, D.H. Kim, B. Lee, E.K. Lee, K.W. Chung, K.M. Moon, M.J. Kim, H.J. An, J.W. Jeong, Y.R. Kim, B.P. Yu, H.Y. Chung, E.J. Jang, D.H. Kim, B. Lee, E. K. Lee, K.W. Chung, K.M. Moon, M.J. Kim, H.J. An, J.W. Jeong, Y.R. Kim, B.P. Yu, H.Y. Chung, Activation of proinflammatory signaling by 4-hydroxynonenal-Src adducts in aged kidneys, Oncotarget 7 (2016) 50864–50874, https://doi.org/10.18632/ONCOTARGET.10854.

[65] P. Zhao, K. Wong, X. Sun, S.M. Reilly, M. Uhm, Z. Liao, Y. Skorobogatko, A.R. Saltiel, TBK1 at the crossroads of inflammation and energy homeostasis in adipose tissue, Cell 172 (2018) 731, https://doi.org/10.1016/J.CELL.2018.01.007.

[66] N. Cianci, M. Subhani, T. Hill, A. Khanna, D. Zheng, A. Sheth, C. Crooks, G.P. Aithal, Prognostic non-invasive biomarkers for all-cause mortality in non-alcoholic fatty liver disease: a systematic review and meta-analysis, World J. Hepatol. 14 (2022) 1025, https://doi.org/10.4254/WJH.V14.I5.1025.

[67] T. Tsuchida, S.L. Friedman, Mechanisms of hepatic stellate cell activation, Nat. Rev. Gastroenterol. Hepatol. 14 (2017) 397–411, https://doi.org/10.1038/NRGASTRO.2017.38.

[68] K. Ikejima, Y. Takei, H. Honda, M. Hirose, M. Yoshikawa, Y.-J. Zhang, T. Lang, T. Fukuda, S. Yamashina, T. Kitamura, N. Sato, Leptin receptor–mediated signaling regulates hepatic fibrogenesis and remodeling of extracellular matrix in the rat, Gastroenterology 122 (2002) 1399–1410, https://doi.org/10.1053/gast.2002.32995.

[69] S.S. Choi, W.K. Syn, G.F. Karaca, A. Omenetti, C.A. Moylan, R.P. Witek, K.M. Agboola, Y. Jung, G.A. Michelotti, A.M. Diehl, Leptin promotes the myofibroblastic phenotype in hepatic stellate cells by activating the Hedgehog pathway, J. Biol. Chem. 285 (2010) 36551–36560, https://doi.org/10.1074/jbc.M110.168542.

[70] P. Mulder, M.C. Morrison, P.Y. Wielinga, W. Van Duyvenvoorde, T. Kooistra, R. Kleemann, Surgical removal of inflamed epididymal white adipose tissue attenuates the development of non-alcoholic steatohepatitis in obesity, Int. J. Obes. 40 (2016) 675–684, https://doi.org/10.1038/ijo.2015.226.

[71] T. Skurk, C. Alberti-Huber, C. Herder, H. Hauner, Relationship between adipocyte size and adipokine expression and secretion, J. Clin. Endocrinol. Metab. 92 (2007) 1023–1033, https://doi.org/10.1210/JC.2006-1055.

[72] A.E. Espinosa De Ycaza, E. Søndergaard, M. Morgan-Bathke, K. Lytle, D.A. Delivanis, P. Ramos, B.G. Carranza Leon, M.D. Jensen, Adipose tissue inflammation is not related to adipose insulin resistance in humans, Diabetes 71 (2022) 381–393, https://doi.org/10.2337/DB21-0609.
[73] M. Małodobra-Mazur, A. Cierzniak, D. Pawełka, K. Kaliszewski, J. Rudnicki, T. Dobosz, Metabolic differences between subcutaneous and visceral adipocytes differentiated with an excess of saturated and monounsaturated fatty acids, Genes (Basel) 11 (2020) 1–16, https://doi.org/10.3390/GENES11091092.
[74] R. Lomonaco, C. Ortiz-Lopez, B. Orsak, A. Webb, J. Hardies, C. Darland, J. Finch, A. Gastaldelli, S. Harrison, F. Tio, K. Cusi, Effect of adipose tissue insulin resistance on metabolic parameters and liver histology in obese patients with nonalcoholic fatty liver disease, Hepatology 55 (2012) 1389–1397, https://doi.org/10.1002/hep.25539.
[75] K.L. Donnelly, C.I. Smith, S.J. Schwarzenberg, J. Jessurun, M.D. Boldt, E.J. Parks, Sources of fatty acids stored in liver and secreted via lipoproteins in patients with nonalcoholic fatty liver disease, J. Clin. Invest. 115 (2005) 1343–1351, https://doi.org/10.1172/JCI23621.
[76] S. Rabot, M. Membrez, A. Bruneau, P. Gerard, T. Harach, M. Moser, F. Raymond, R. Mansourian, C.J. Chou, Germ-free C57BL/6J mice are resistant to high-fat-diet-induced insulin resistance and have altered cholesterol metabolism, Faseb. J. 24 (2010) 4948–4959, https://doi.org/10.1096/fj.10-164921.
[77] F. Bäckhed, J.K. Manchester, C.F. Semenkovich, J.I. Gordon, Mechanisms underlying the resistance to diet-induced obesity in germ-free mice, Proc. Natl. Acad. Sci. USA 104 (2007) 979–984, https://doi.org/10.1073/pnas.0605374104.
[78] J. Aron-Wisnewsky, J. Doré, K. Clement, The importance of the gut microbiota after bariatric surgery, Nat. Rev. Gastroenterol. Hepatol. 9 (2012) 590–598.
[79] R.M. Carr, A.E. Reid, FXR agonists as therapeutic agents for non-alcoholic fatty liver disease, Curr. Atherosclerosis Rep. 17 (2015).
[80] G. den Besten, K. Lange, R. Havinga, T.H. van Dijk, A. Gerding, K. van Eunen, M. Muller, A.K. Groen, G.J. Hooiveld, B.M. Bakker, D.-J. Reijngoud, Gut-derived short-chain fatty acids are vividly assimilated into host carbohydrates and lipids, AJP Gastrointest Liver Physiol. 305 (2013) G900–G910, https://doi.org/10.1152/ajpgi.00265.2013.
[81] G. den Besten, K. van Eunen, A.K. Groen, K. Venema, D.-J. Reijngoud, B.M. Bakker, The role of short-chain fatty acids in the interplay between diet, gut microbiota, and host energy metabolism, J. Lipid Res. 54 (2013) 2325–2340, https://doi.org/10.1194/jlr.R036012.
[82] L. Craven, A. Rahman, S. Nair Parvathy, M. Beaton, J. Silverman, K. Qumosani, I. Hramiak, R. Hegele, T. Joy, J. Meddings, B. Urquhart, R. Harvie, C. McKenzie, K. Summers, G. Reid, J.P. Burton, M. Silverman, Allogenic fecal microbiota transplantation in patients with nonalcoholic fatty liver disease improves abnormal small intestinal permeability: a randomized control trial, Am. J. Gastroenterol. 115 (2020) 1055–1065, https://doi.org/10.14309/AJG.0000000000000661.
[83] L. Miele, V. Valenza, G. La Torre, M. Montalto, G. Cammarota, R. Ricci, R. Mascianà, A. Forgione, M.L. Gabrieli, G. Perotti, F.M. Vecchio, G. Rapaccini, G. Gasbarrini, C.P. Day, A. Grieco, Increased intestinal permeability and tight junction alterations in nonalcoholic fatty liver disease, Hepatology 49 (2009) 1877–1887, https://doi.org/10.1002/hep.22848.
[84] P. Mulder, M.C. Morrison, L. Verschuren, W. Liang, J.H. Van Bockel, T. Kooistra, P.Y. Wielinga, R. Kleemann, Reduction of obesity-associated white adipose tissue inflammation by rosiglitazone is associated with reduced non-alcoholic fatty liver disease in LDLr-deficient mice, Sci. Rep. 6 (2016), https://doi.org/10.1038/SREP31542.
[85] K. Salic, R. Kleemann, C. Wilkins-Port, J. McNulty, L. Verschuren, M. Palmer, Apical sodium-dependent bile acid transporter inhibition with volixibat improves metabolic aspects and components of non-alcoholic steatohepatitis in Ldlr-/-.Leiden mice, PLoS One 14 (2019), https://doi.org/10.1371/JOURNAL.PONE.0218459.
[86] M.C. Morrison, P. Mulder, K. Salic, J. Verheij, W. Liang, W. van Duyvenvoorde, A. Menke, T. Kooistra, R. Kleemann, P.Y. Wielinga, Intervention with a caspase-1 inhibitor reduces obesity-associated hyperinsulinemia, non-alcoholic steatohepatitis and hepatic fibrosis in LDLR−/−.Leiden mice, Int. J. Obes. 40 (2016) 1416–1423, https://doi.org/10.1038/ijo.2016.74.